Prediction of Soot Formation in Laminar Opposed Diffusion Flame with Detailed and Reduced Reaction Mechanisms

A Thesis
Presented to
The Academic Faculty

by

Hojoon Chang

In Partial Fulfillment
of the Requirements for the Degree
Master of Science

School of Aerospace Engineering
Georgia Institute of Technology
August 2004

Prediction of Soot Formation in Laminar Opposed Diffusion Flame with Detailed and Reduced Reaction Mechanisms

Approved by:

Professor Suresh Menon, Committee Chair
School of Aerospace

Professor Jechiel Jagoda
School of Aerospace

Professor Jerry Seitzman
School of Aerospace

Date Approved: November 2004

To my parents

TABLE OF CONTENTS

LIST OF TABLES

LIST OF FIGURES

SUMMARY

The present work focuses on a computational study of a simplified soot model to predict soot production and destruction in methane/oxidizer(O_2 and N_2) and ethylene/air flames using a one-dimensional laminar opposed diffusion flame setup. Two different detailed reaction mechanisms (361 reactions & 61 species for methane/oxidizer flame and 527 reactions & 99 species for ethylene/air flame) are used to validate the simplified soot model in each flame. The effects of strain rate and oxygen content on the soot production and destruction are studied, and the soot related properties such as soot volume fraction, particle number density and particle diameter are compared with published results. The results show reasonable agreement with data and that the soot volume fraction decreases with higher strain rate and lower oxygen content. The simplified soot model has also been used with two reduced reaction mechanisms (12-step, 16-species for methane flame and 20-species for ethylene flame) since such reduced mechanisms are computationally more efficient for practical application. The profiles of the physical properties and the major species are in excellent agreement with the results using the detailed reaction mechanisms. However, minor hydrocarbon-species such as acetylene (C_2H_2) that is the primary pyrolysis species in the simplified soot model is significantly over predicted and this, in turn, results in an over-prediction of soot production. Finally, the reduced reaction mechanism is modified to get more accurate prediction of the minor hydrocarbon-species. The modified reduced reaction mechanism shows that the soot prediction can be improved by improving the predictions of the key minor species.

CHAPTER I

INTRODUCTION

Soot particles are formed from almost every combustion system from candles to complex combustion devices, such as engines, furnaces, etc. The soot particles during combustion cause a flame to be luminous and enhance heat transfer by radiation. Nowadays, however, it has caused much concern for health and environmental reasons because of its carcinogenic nature, and new government regulations require that it should be minimized or eliminated from combustion devices. Therefore, accurate prediction of soot during the combustion process will help us to develop the methods to reduce it.

Soot is produced from incomplete combustion, meaning that the oxidizer is not sufficient to burn hydrocarbon locally. A detailed soot mechanism is still unknown because soot formation is a complex mechanism; however, the identical chemical characteristics of soot irrespective of a fuel and flame type [12] imply that it is possible to generalize the chemical mechanisms for soot formation and destruction. From past works [12, 3, 35], it is generally agreed that these generalized mechanisms include (i) formation of precursor species, (ii) particle inception, (iii) surface growth and particle agglomeration and (iv) particle oxidation. Conceptually, in the first step, formation of precursor species, the important role is played by Polycyclic Aromatic Hydrocarbons (PAH) which are intermediates between an original fuel molecule and a primary soot particle. If the fuel is non-aromatic, the precursors experience cyclization to create an aromatic ring, and then the ring structure is developed into PAH by the addition of alkyl groups, which are groups of carbon and hydrogen atoms derived from an alkane molecule by removing a hydrogen atom. The PAH then becomes small soot particles of a critical size (initial particle size about 400 $\dot{A}$ [16] or 3,000-10,000 atomic mass units [35]) by both chemical means and coagulation in the second step, particle inception. This step is a kind of gaseous-solid phase transition, and then the particles of the critical size are physically identified as solid. The small soot particles then undergo surface growth

by absorbing surrounding gas phase molecules and particle agglomeration by attracting each other. The size of soot particles is rapidly increased by surface growth and particle agglomeration, and this step determines the final size of the soot particles. Finally, the soot particles formed in the interior of the flame can get oxidized by O_2 and OH [11] if they pass through the flame.

Early research groups have measured the soot formation and destruction in different conditions, such as Bunsen-type flames [30, 33], flat flames [23], stirred reactor [43, 2] for premixed combustion, co-flowing Wolfhard-Parker burners [42, 22], axisymetric diffusion flame [27], and a counter-flow diffusion flame [6, 36, 37, 38]. From past experimental works, temperature plays the most dominant role in the soot formation and destruction because the soot formation mechanism is assumed to be related to high activation energy step. Santoro et al. [26] who used a laminar ethane/air co-annular diffusion flame showed that the major soot formation occurs near fuel side of the flame and soot is formed over a limited range of temperatures (1300 K - 1600 K). In addition to the temperature, several other physical characteristics, such as fuel flow rate [26], pressure [4], fuel structure [12], and oxygen index [36], also affect soot formation and destruction.

As the experimental approaches have attempted to address nature of soot, several numerical modeling have been proposed to figure it out, too. Earlier research groups [34, 13, 24] have proposed several models that have a very simple description of the gas-phase chemistry-soot interaction in different conditions, such as premixed flames, counter-flowing diffusion flames, or shock tube. Their models were consistent with experiments if the experimental conditions were similar to the data which was used to calibrate the models. However, the application of these models in different conditions had significant errors because these models had a very simple reaction mechanism, and the formation of soot was directly linked to the fuel concentration or mixture fraction. Therefore, several research groups (Frenklach et al. [7, 8], Lindstedt et al. [17, 18, 19], Brookes et al. [4, 5]) have suggested more generalized models applicable under several conditions. Extended reaction mechanisms have been used for these generalized models. These models usually assume that soot formation process is dependent upon the fuel breakdown process. Frenklach et al. [7, 8] used method of moments

based on the particle size distribution function (PDF) with a 337-reaction, 70-species mechanism. In their model, the first aromatic ring is formed via C_2H_2 / $n-C_4H_3$ or $n-C_4H_5$ reactions. Their results are in quantitative agreement with experimental results from several laminar premixed hydrocarbon flames. However, Miller et al. [21] showed that the reactions of $n-C_4H_3$ and $n-C_4H_5$ are not effective in producing aromatic compounds because only small quantities of these isomers are present in a flame and it is impossible to distinguish between $i-C_4H_3$ & $i-C_4H_5$, which are more stable isomers, and $n-C_4H_3$ & $n-C_4H_5$ by a mass spectrometer. They suggested C_3H_3 reactions instead of $n-C_4H_3$ or $n-C_4H_5$ reactions as the most likely reactions producing the first ring. Another group, Lindstedt et al. [17, 19] suggested a simplified reaction mechanism that includes soot nucleation, surface growth, particle coagulation, and finally destruction via combustion. They assumed that soot formation is dependent upon the breakdown path of the fuel and the presence of pyrolysis products, such as acetylene, and polyunsaturated cyclical hydrocarbons, such as benzene. They thought that the presence of pyrolysis products is a crucial feature of the soot formation process because soot nucleation and surface growth are linked to the gas phase by presuming pyrolysis products. Beltrame et al. [1] used Lindstedt's model with extended reaction mechanism which includes Miller's C_3H_3 reactions for methane-oxygen enriched diffusion flames.

The present work uses benzene for a detailed reaction mechanism and acetylene for a detailed and two reduced reaction mechanisms as the main pyrolysis products that lead to the soot formation process. Once the soot particles have been made, these particles experience surface growth, particle agglomeration and finally destruction by oxidation.

The all reaction mechanisms that are used in the present work are based on GRI-Mech. The one of the detailed reaction mechanisms was developed by extending GRI-Mech 2.11 up to C_6 chemistry especially for C_1-C_6 chemical kinetic model [1], and the other detailed reaction mechanism was developed by modifying GRI-Mech 1.2 to describe acetylene and ethylene oxidation in flame more accurately since GRI-Mech was optimized for natural-gas combustion [41]. The reduced reaction mechanisms are consisting of a 12-step, 16-species for methane flame and a 20-species for ethylene flame, which were developed from GRI-MECH

1.2 [32].

The simplified soot model which uses benzene or acetylene as the main pyrolysis products with all of the reaction mechanisms consists of a four-step reaction and employs two-equations: **conservation of soot mass fraction** and **soot particle number density**. The simplified soot model based on the detailed reaction mechanisms is validated by simulating and comparing cases available in the literatures. Then, the numerical data from the simplified soot model with the reduced reaction mechanisms are compared to the numerical data from the simplified soot model with the detailed reaction mechanisms.

CHAPTER II

OBJECTIVES

1. Evaluate accuracy of the simplified soot model with the detailed reaction mechanisms.

   Laminar opposed diffusion flame code is modified to include the simplified soot model. The modified code calculates temperature, flow velocity, density, n-species molar fractions, soot volume fraction, soot number density and soot particle diameter using the detailed reaction mechanisms, and then the data are compared with experimental results.

2. Study effects of strain rate and oxygen content on soot production using laminar opposed jet diffusion flame set up.

   The modified code is run on the several strain rates and oxygen contents, and the maximum soot volume fractions and profiles are examined.

3. Evaluate accuracy of the simplified soot model with the reduced reaction mechanisms.

   The simplified soot model is combined with the reduced reaction mechanisms and the numerical data based on the reduced and the detailed reaction mechanisms are compared with each other.

4. Evaluate accuracy of the simplified soot model with the modified reduced reaction mechanism.

   The simplified soot model is combined with the modified reduced reaction mechanism and the numerical data based on the modified reduced and the detailed reaction mechanisms are compared with each other.

CHAPTER III

NUMERICAL MODELS

3.1 Simplified Soot Model using Benzene

Beltrame et al. [1] presented a simplified soot model based on the models developed earlier by Lindstedt et al. [19]. It consisted of four reactions and nine species including soot, and they used benzene as the main pyrolysis product for the detailed reaction mechanism in Chapter 3.3.1. The nine species are C_6H_6, C_6H_5, H_2, H, O_2, C_2H_2, CO, OH and soot. Even though soot is not a chemical species, the simplified soot model uses it as a species.

Soot nucleation is by the following reaction:

$$\begin{aligned} C_6H_6 + C_6H_5 &\Rightarrow 12C_s + 5H_2 + H \qquad (1) \\ R_1 &= k_1(T)[C_6H_6][C_6H_5] \\ k_1 &= 7.00\text{E+}09 \end{aligned}$$

where C_s represents the number of carbon atoms in soot. Initially, the rate constant of this reaction was adjusted by Beltrame et al. [1] to predict the soot volume fraction for the methane-air flame with a strain rate of 20 s^{-1} in opposed diffusion flame. They assumed that this reaction has no activation energy, so only the pre-exponential factor should be fixed.

Soot surface growth is due to the absorption of acetylene by the soot particle.

$$\begin{aligned} C_2H_2 + nC_s &\Rightarrow (n+2)C_s + H_2 \qquad (2) \\ R_2 &= k_2(T)f(A_s)[C_2H_2] \\ k_2 &= 7.00\text{E-}07e^{\frac{24{,}043}{R_uT}} \end{aligned}$$

where $f(A_s)$ is a function of the total surface area and R_u is universal gas constant, 1.98588 $cal/mole/K$.

If we follow Lindstedt et al.'s assumption [19] that the reaction rate is proportional to the number of soot particles but independent of the surface area, the function of the total surface area is:

$$f(A_s) = \frac{A_s}{a_p} = [\rho N_s] \tag{3}$$

Here, A_s is the soot surface area, a_p is the surface area of an individual particle, ρ is the density and N_s is the soot number density per unit mass [1/g].

Soot oxidation is related to species O_2 and OH. Lindstedt et al. [19] explained oxidation as:

$$\begin{aligned} C_s + \frac{1}{2}O_2 &\Rightarrow CO \qquad (4)\\ R_3 &= k_3(T)A_s[O_2] \\ k_3 &= 1.00\text{E+}06T^{0.5}e^{\frac{38{,}970}{R_uT}} \end{aligned}$$

$$\begin{aligned} C_s + OH &\Rightarrow CO + H \qquad (5)\\ R_4 &= k_4(T)A_s[OH] \\ k_4 &= 1.00\text{E+}06T^{0.5}e^{\frac{38{,}970}{R_uT}} \end{aligned}$$

Soot particles were assumed to be spherical with the diameter as a function of the axial coordinate x only. With the spherical particle assumption, the particle properties are as follows [19]:

$$d_p = \left(\frac{6}{\pi}\frac{\rho}{\rho_s}\frac{Y_s}{[\rho N_s]}\right)^{\frac{1}{3}} \tag{6}$$

$$a_p = \pi d_p^2 \tag{7}$$

$$A_s = \pi d_p^2[\rho N_s] \tag{8}$$

where d_p is the particle diameter, a_p is the surface area of an individual particle, A_s is the soot surface area, ρ is the density, N_s is the soot number density per unit mass, and Y_s is the soot mass fraction. Soot density, ρ_s is assumed to be 2 g/cm^3.

If the particle diameter d_p is almost zero diameter when the soot mass fraction Y_s is small as compared with the soot particle number density ρN_s, the soot surface area A_s

and the surface area a_p of an individual particle are small, too. Then this makes the soot oxidation rates are significantly small, but soot nucleation and surface growth rate are not affected by the zero diameter since both rates are independent of the soot particle diameter in Equation 1 and 2.

3.2 Simplified Soot Model using Acetylene

Kronenburg et al. [14] showed another simplified soot model based on the models developed earlier by Lindstedt et al. [19]. Their simplified soot model used acetylene, C_2H_2, as the main pyrolysis product. Therefore, their model could not reflect the effects of other species that are commoly associated with soot formation, such as C_6H_6, C_4H_2, and C_4H_6 which was indicated by Smyth et al. [29]. Their model consists of four reactions and seven species including soot, and the seven species are $H_2, H, O_2, C_2H_2, CO, OH$, and soot. Again, soot is considered a chemical species.

The four reaction steps and the reaction rates are shown below:

$$\begin{aligned} \textbf{Soot nucleation: } C_2H_2 &\Rightarrow 2C_s + H_2 \\ R_1 &= k_1(T)[C_2H_2] \\ k_1 &= 0.63\text{E+}04e^{\frac{21{,}000}{T}} \end{aligned} \tag{9}$$

$$\begin{aligned} \textbf{Soot surface growth: } C_2H_2 + nC_s &\Rightarrow (n+2)C_s + H_2 \\ R_2 &= k_2(T)f(A_s)[C_2H_2] \\ k_2 &= 0.75\text{E+}03e^{\frac{12{,}000}{T}} \end{aligned} \tag{10}$$

$$\begin{aligned} \textbf{Soot oxidation by } O_2\textbf{: } C_s + \frac{1}{2}O_2 &\Rightarrow CO \\ R_3 &= k_3(T)A_s[O_2] \\ k_3 &= 7.15\text{E+}02T^{0.5}e^{\frac{19{,}800}{T}} \end{aligned} \tag{11}$$

$$\begin{aligned} \textbf{Soot oxidation by } OH\textbf{: } C_s + OH &\Rightarrow CO + H \\ R_4 &= k_4(T)A_s[OH] \\ k_4 &= 0.36T^{0.5} \end{aligned} \tag{12}$$

where $f(A_s)$ is a function of the total surface area and units are in K, $kmol$, m, and s.

Kronenburg et al. [14] assumed that the reactivity is simply proportional to the local surface area and the acetylene concentration. Then, the function of the total surface area is:

$$f(A_s) = A_s \tag{13}$$

Other properties such as d_p, a_p, and A_s have the same form as defined in Section 3.1.

3.3 Detailed Reaction Mechanism

3.3.1 Beltrame et al.'s reaction mechanism

Beltrame et al. [1] 's detailed reaction mechanism of GRI-MECH 2.11 and the extended soot relevant reactions includes 361 reactions and 61 species, with a focus on $C_1 - C_6$ chemistry. The extended reactions are shown in Table A1 – A1 of the Appendix, and the 61 species are:

$$H_2, H, O, O_2, OH, H_2O, HO_2, H_2O_2, C, CH, CH_2, CH_2(S), CH_3, CH_4, CO, CO_2$$

$$HCO, CH_2O, CH_2OH, CH_3O, CH_3OH, C_2H, C_2H_2, C_2H_3, NH_2, NH_3, NNH$$

$$NO, NO_2, HNO, CN, HCN, H_2CN, HCNN, HCNO, HOCN, HNCO, NCO$$

$$N_2, AR, C_2H_4, C_2H_5, C_2H_6, HCCO, CH_2CO, HCCOH, N, NH, C_3H_3, C_3H_2,$$

$$C_3H_4, pC_3H_4, nC_4H_3, C_4H_4, C_6H_5, C_6H_6, C_3H_4CY, iC_4H_3, nC_4H_5, iC_4H_5.$$

3.3.2 Wang et al.'s reaction mechanism

Wang et al. [41] suggested a detailed reaction mechanism which consists of 527 reactions and 99 chemical species. It is partly based on GRI-Mech 1.2 [10] and extended to describe acetylene and ethylene oxidation because the GRI-Mech was optimized for natural-gas combustion. The detailed reaction mechanism and thermochemical properties are given in the reference [41].

3.4 Reduced Reaction Mechanism

Although the detailed reaction mechanism provides accurate results, it is not considered practical because the number of species and reactions are too large. Accordingly, many research groups have developed reduced reaction mechanisms using various simplifications that solve a smaller set of species equations.

3.4.1 12-step, 16-species for Methane Flame

Sung et al. [32] have presented a 12-step, 16-species reduced reaction mechanism that includes up to C_2 species. It is shown in Table A2 of the Appendix, and the 16 species are:

$$H_2, H, O_2, OH, H_2O, HO_2, H_2O_2, CH_3, CH_4, CO, CO_2, CH_2O, C_2H_2, C_2H_4, C_2H_6, N_2$$

3.4.2 20-species for Ethylene Flame

The 20-species reduced reaction mechanism was used for ethylene/air flame. The 20 species are shown below:

$$H_2, H, O, O_2, OH, H_2O, HO_2, H_2O_2, CH_3, CH_4, CO, CO_2, CH_2O, CH_3OH, C_2H_2,$$
$$C_2H_4, CH_2CO, C_3H_6, aC_3H_5, N_2$$

It should be noted that these reduced mechanisms were designed mainly for gas-phase methane/air or ethylene/air reactions and the goal here is to determine if they can be used to study soot formation as well.

CHAPTER IV

FORMULATION

Laminar Opposed Diffusion Flame Modelling

The governing equations are the steady-state conservation equations for mass, momentum, energy and n-species. These equations are assumed that the temperature, T, and species mass fractions, Y_i, are functions of x alone, and the pressure, P, is constant through out the flow field under the low-Mach number approximation. The pressure gradient terms, however, still appear in the momentum equations. The buoyancy force is ignored in the momentum equations. These conservation equations in cylindrical coordinates are [35]:

$$\frac{\partial}{\partial x}(r\rho u) + \frac{\partial}{\partial r}(r\rho v) = 0 \tag{14}$$

$$\frac{\partial}{\partial x}(r\rho uu) + \frac{\partial}{\partial r}(r\rho vu) = \frac{\partial}{\partial r}(r\tau_{rx}) + r\frac{\partial \tau_{xx}}{\partial x} - r\frac{\partial P}{\partial x} \tag{15}$$

$$\frac{\partial}{\partial x}(r\rho uv) + \frac{\partial}{\partial r}(r\rho vv) = \frac{\partial}{\partial r}(r\tau_{rr}) + r\frac{\partial \tau_{rx}}{\partial x} - r\frac{\partial P}{\partial r} \tag{16}$$

$$\rho u c_p \frac{dT}{dx} - \frac{d}{dx}(k\frac{dT}{dx}) + \sum_{i=1}^{N} \rho Y_i u_{i,diff} c_{p,i} \frac{dT}{dx} - \sum_{i=1}^{N} h_i \dot{w}_i MW_i = 0 \tag{17}$$

$$\rho u \frac{dY_i}{dx} + \frac{d}{dx}(\rho Y_i u_{i,diff}) - \dot{w}_i MW_i = 0 \tag{18}$$

where u and v are the axial and radial velocity components, respectively. ρ is the density and c_p is the specific heat at constant pressure. h_i is absolute enthalpy of species i, $\dot{w}_i$ is net production rate of species i, and MW_i is the molecular weight of species i. The viscous stresses terms are

$$\tau_{xx} = 2\mu\left[\frac{\partial u}{\partial x} - \frac{1}{3}(\overrightarrow{\nabla}\cdot\overrightarrow{V})\right] \tag{19}$$

$$\tau_{rr} = 2\mu\left[\frac{\partial v}{\partial r} - \frac{1}{3}(\overrightarrow{\nabla}\cdot\overrightarrow{V})\right] \tag{20}$$

$$\tau_{rx} = \mu\left[2\frac{\partial u}{\partial r} + \frac{\partial v}{\partial x}\right] \tag{21}$$

$$\overrightarrow{\nabla}\cdot\overrightarrow{V} = \frac{1}{r}\frac{\partial}{\partial r}(rv) + \frac{\partial u}{\partial x} \tag{22}$$

where μ is the fluid viscosity. The diffusion velocities of species i is given by

$$u_{i,diff} = \frac{1}{\chi_i MW_{mix}} \sum_{j=1}^{N} MW_j D_{ij} \frac{d\chi_j}{dx} - \frac{D_i^T}{\rho Y_i} \frac{1}{T} \frac{dT}{dx} \tag{23}$$

where χ_i is the species molar fraction, MW_{mix} is the molecular weight of the mixture, D_{ij} is the ordinary multi-component diffusion coefficient and D_i^T is the thermal diffusion coefficient. Boundary conditions of the mixture composition, temperature, and the inlet velocity are specified at both nozzle exits. The inlet velocities are calculated based on the strain rate, which is the potential flow velocity gradient in the oxidizer stream, and is defined as follow:

$$a = -\frac{\partial u_\infty}{\partial x} \tag{24}$$

Two additional equations for the simplified soot model are added to the governing equations in a form similar to Equation (18). One is **conservation of soot mass fraction** (25), and the other is **conservation of soot particle number density** (26). These are

$$\rho u \frac{dY_s}{dx} + \frac{d}{dx}(\rho Y_s u_{Y_s,diff}) = \dot{w}_s MW_s \quad \text{, where} \quad u_{Y_s,diff} = -\frac{D_{Y_s}}{Y_s} \frac{dY_s}{dx} \tag{25}$$

$$\rho u \frac{dN_s}{dx} + \frac{d}{dx}(\rho N_s u_{N_s,diff}) = \dot{w}_{N_s} \quad \text{, where} \quad u_{N_s,diff} = -\frac{D_{N_s}}{N_s} \frac{dN_s}{dx} \tag{26}$$

where $u_{Y_s,diff}$ and $u_{N_s,diff}$ are, respectively, the diffusion velocities for the soot mass fraction and the soot number density. MW_s is the molecular weight of soot and it is assumed to be 12.011 $g/mole$. Also, $\dot{w}_s$ and $\dot{w}_{N_s}$ are, respectively, the source terms of the soot mass fraction and the soot number density. D_{Y_s} and D_{N_s} are, respectively, the diffusion coefficients for soot mass fraction and soot number density.

Beltrame et al. [1] mentioned that soot particles are considered too large to have appreciable diffusion velocities and they are only convected at local gas velocities. Accordingly, the above equations (25, 26) are reduced to:

$$\rho u \frac{dY_s}{dx} = \dot{w}_s MW_s \tag{27}$$

$$\rho u \frac{dN_s}{dx} = \dot{w}_{N_s} \tag{28}$$

The RHS of two equations are source terms and physically imply:

$$\dot{w}_s MW_s = Formation - Oxidation \quad (29)$$

$$\dot{w}_{N_s} = Formation - Agglomeration \quad (30)$$

and are expressed as follows:

Detailed Reaction Mechanism

$$\dot{w}_s MW_s = (12R_1 + 2R_2 - R_3 - R_4)MW_s \quad (31)$$

$$\dot{w}_{N_s} = 12R_1 \frac{N_{AV}}{C_{min}} - 2C_a d_p^{0.5} (\frac{6k_B T}{\rho_s})^{0.5} [\rho N_s]^2 \quad (32)$$

Reduced Reaction Mechanism

$$\dot{w}_s MW_s = (2R_1 + 2R_2 - R_3 - R_4)MW_s \quad (33)$$

$$\dot{w}_{N_s} = 2R_1 \frac{N_{AV}}{C_{min}} - 2C_a d_p^{0.5} (\frac{6k_B T}{\rho_s})^{0.5} [\rho N_s]^2 \quad (34)$$

where N_{AV} is Avogadro number, 6.022136E+23 $molecules/mol$, C_{min} is the number of carbon atoms in the incipient carbon particle, 100, C_a is the agglomeration rate constant, 9.0, and k_B is the Boltzmann constant, 1.38E-16 $g \cdot cm^2/K/s^2/molecules$. In Equation (29), agglomeration does not affect the source term of the soot mass fraction because mass of each soot particle is conserved after agglomeration. Oxidation, however, has influence on the soot particle number density by reducing the soot mass fraction and the soot particle diameter, but the present work assums that it does not directly affect in the source term of the soot particle number density in Equation (30). This is consistent with earlier studies [17, 19].

The soot volume fraction can be calculated as:

$$f_v = \frac{\rho}{\rho_s} Y_s = (\frac{\pi}{6} d_p^3)[\rho N_s] \quad (35)$$

CHAPTER V

NUMERICAL RESULTS AND DISCUSSION

The numerical computations are performed using a one-dimensional laminar opposed diffusion flame setup similar to the OPPDIF code, which is a part of CHEMKIN [20]. This code solves for the temperature, species mass fraction, axial and radial velocity components and radial pressure gradient in the steady state. A schematic drawing of simulation configuration is shown in Figure 1.

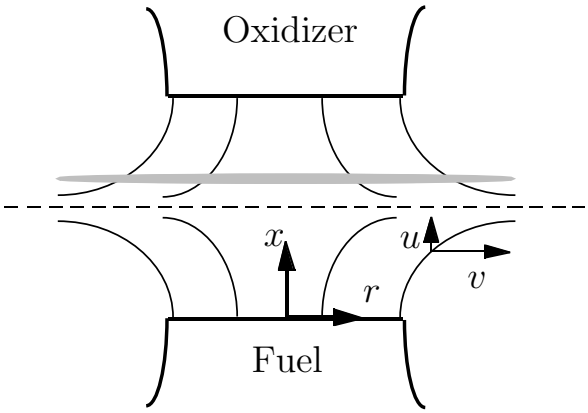

Figure 1: Simulation configuration

5.1 Validation of Simplified Soot Model using Benzene with Beltrame et al.'s detailed reaction mechanism in Methane Flame

In these computation, the fuel(methane) and oxidizer(oxygen/nitrogen mixture) are supplied from two opposing nozzles set a distance of 2 cm apart. The initial temperatures of both sides are 300 K, and the strain rate is 20 s^{-1}. The nozzle velocities are calculated based on the strain rate. The numerical results are compared to the experimental results provided by Beltrame et al. [1].

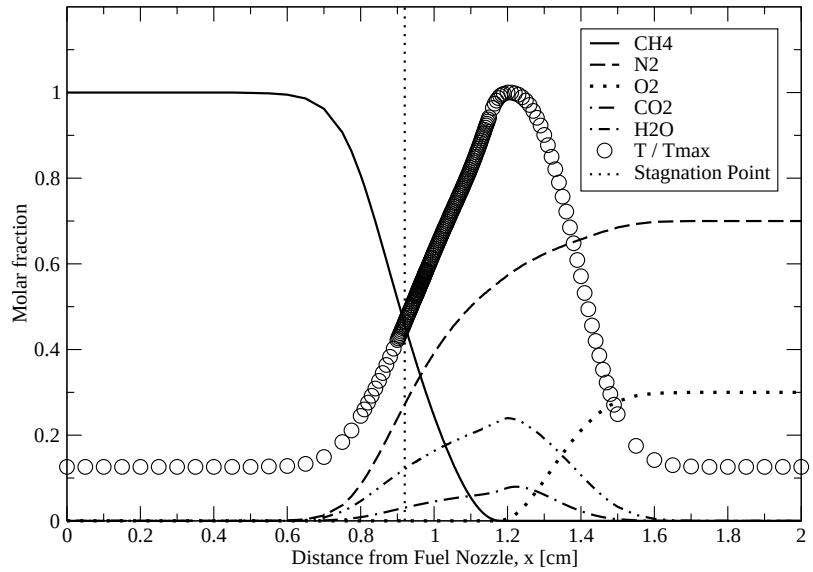

Figure 2: Computed temperature and major species profiles for methane / 30% oxygen flame. Strain rate is 20 s^{-1}.

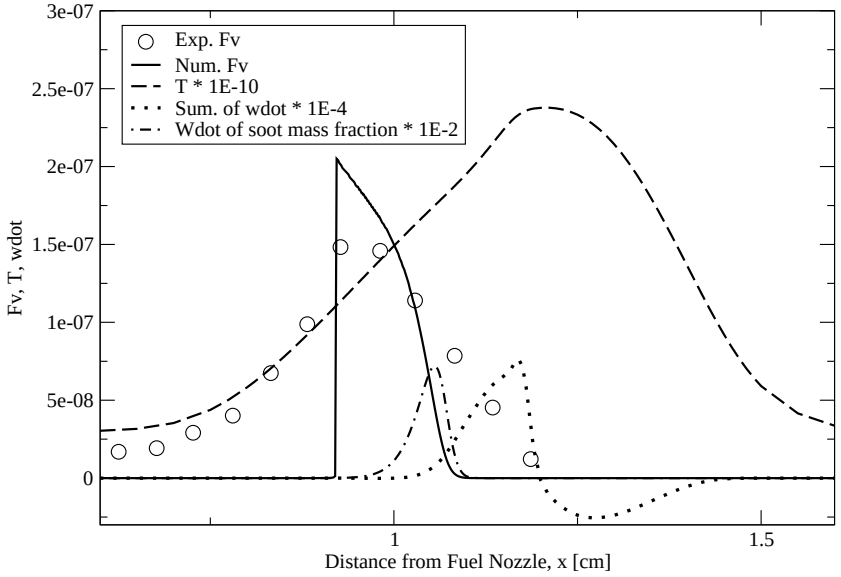

Figure 3: Numerical (solid line) and experimental (symbol) soot volume fractions for methane / 30% oxygen flame. Strain rate is 20 s^{-1}.

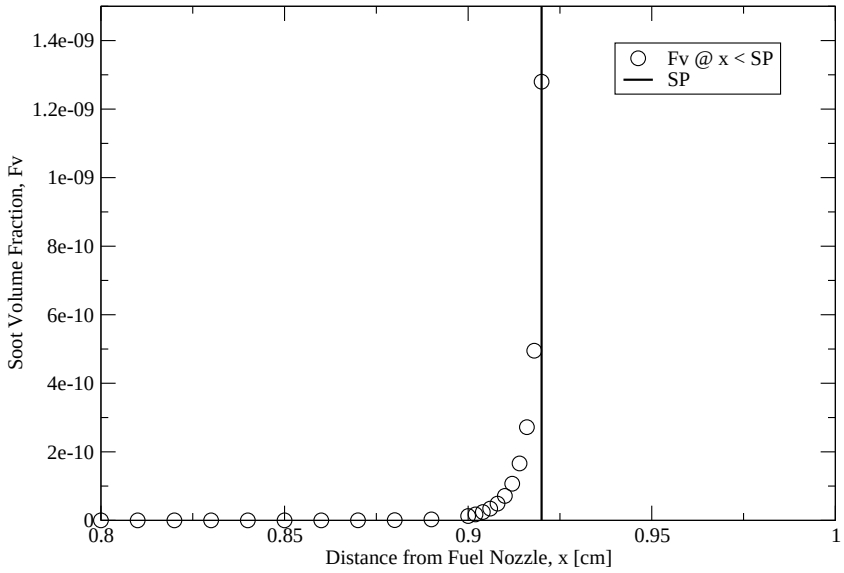

Figure 4: Numerical soot volume fraction before SP. SP stands for Stagnation Point

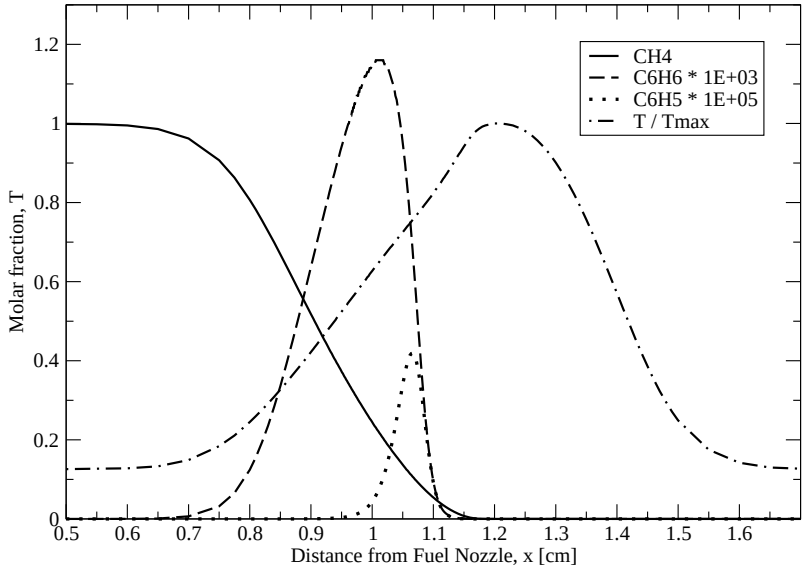

Figure 5: Temperature and molar fractions of CH_4, C_6H_6, and C_6H_5 for methane / 30% oxygen flame. Strain rate is 20 s^{-1}.

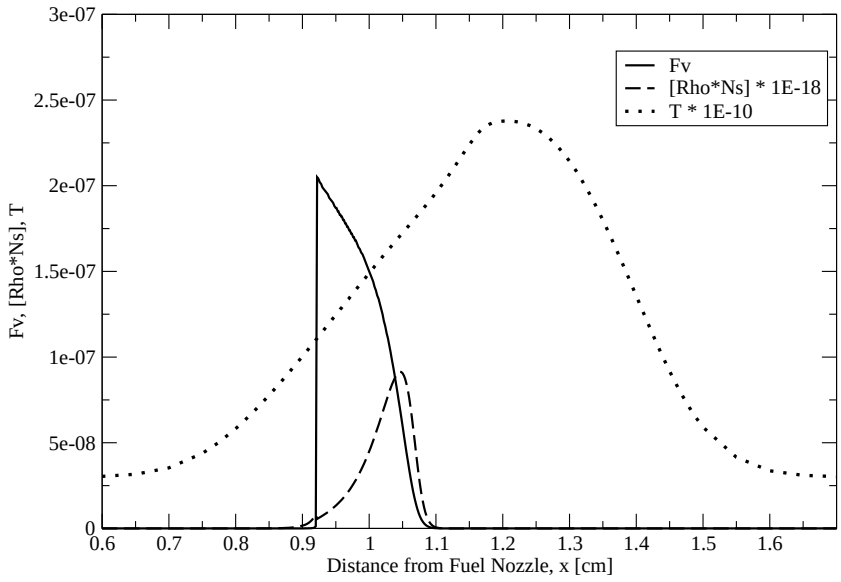

Figure 6: Profiles of soot volume fraction, soot particle number density and temperature for methane / 30% oxygen flame. Strain rate is 20 s^{-1}.

Figure 2 shows molar fractions of major species with temperature and stagnation point. The fuel (CH_4) and oxidizer (30% O_2 & 70% N_2) are supplied from left and right side nozzles and destroyed near the flame. On the other hand, CO_2 and H_2O are produced near the flame as products. The maximum temperature is $2378K$ at $x = 1.21$ cm, and the stagnation point is at 0.920 cm. Figure 3 shows the profiles of the experimental and numerical soot volume fractions along with the profiles of temperature and production rate of soot mass fraction and summation of all species that are showing a flame location. The fuel comes from the left side nozzle and reaches the stagnation point (SP) by convection and passes through the SP by diffusion only. The diffused fuel goes through the high temperature region, and it breaks down to the main pyrolysis products, C_6H_6 and C_6H_5. The profiles of fuel and main pyrolysis products are shown in Figure 5. In the high temperature region, the main pyrolysis products are transformed into PAH, and finally soot inception occurs.

From Figure 6, the soot inception region, where the soot particle number density [ρN_s] increases from flame, is shown to be between 1.05 cm and 1.10 cm, and the soot surface growth occurs between the SP and the soot inception region, where the soot particle number density is decreased by particle agglomeration. Soot particles, which are formed in the soot

inception zone, are moved back to the SP by the gas flow coming from the oxidizer nozzle. Therefore, the numerical soot volume fraction has a peak near the SP. The peak value of the soot volume fraction is consistent with the experimental results, with a difference of 0.5E-07 in Figure 3. However, in Figure 3, the soot volume fraction in the oxidizer side of the SP is under-predicted, and the soot volume fraction in the fuel side of the SP is also less than the experimental results.

Figure 4 shows the soot volume fraction before SP. The maximum soot volume fraction, is 1.28E-09 at x = 0.92 cm, but before SP the soot volume fraction is two orders less than the maximum soot volume (which is 2.05E-07 at x = 0.922 cm) right after SP. These errors can be explained by the lack of soot particle diffusion in the present numerical model, and the effect of upwind differencing, which uses the sign of the velocity to choose the direction of spatial differencing. In counter-flow diffusion flames, all elements in the fuel stream reach the flame front only by molecular diffusion across the SP. The soot particles form only on the fuel side of the flame front, and then are convected back towards the stagnation streamline by convection of local gas velocities. But for young soot particles (with smaller particle diameter), the diffusion can be somewhat larger, and this effect is not included in the modelling primarily because it is difficult to determine a diffusion coefficient for soot particles. Soot diffusion modelling remains an unsolved problem.

Table 1: Peak values of soot volume fraction as a function of oxygen content and strain rate

	Experimental results			Numerical calculations		
Strain rate $[s^{-1}]$	21%	30%	50%	21%	30%	50%
10	0.6E-07			1.09E-07		
20	0.30E-07	1.47E-07	1.77E-07	0.55E-07	2.09E-07	3.19E-07
30			1.3E-07			2.70E-07
40			1.2E-07			2.29E-07

Table 1 and Figure 7 compare the peak values of soot volume fraction at the oxygen contents of 21%, 30%, and 50% with various strain rates. The experimental results were

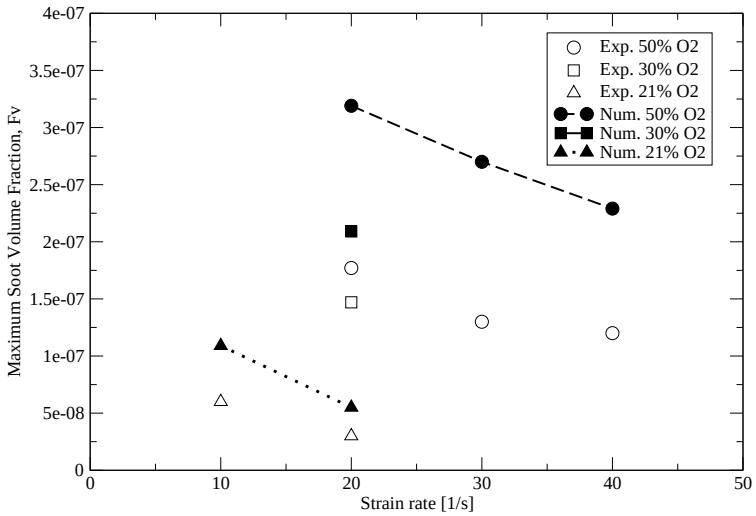

Figure 7: Maximum soot volume fraction as a function of oxygen content in the oxidizer and strain rate

measured by Beltrame et al. [1]. The peak values of the lower oxygen content show small discrepancy with the experimental results, but the difference between experiment and numerical calculation increases as the oxidizer content increases.

Table 2: Maximum temperature, soot particle number density and molar fraction of the main pyrolysis species for various oxygen contents in oxidizer (strain rate 20 s^{-1})

Oxygen contents	Maximum temperature	Maximum soot number density	Maximum molar fraction		
			C_2H_2	C_6H_6	C_6H_5
50% O_2	2742K	7.53E+10	1.22E-02	1.05E-03	3.47E-06
30% O_2	2378K	9.14E+10	9.18E-03	1.16E-03	4.19E-06
21% O_2	2058K	5.54E+10	4.60E-03	6.74E-04	2.60E-06

In Figure 7, the soot volume fraction increases when the oxygen content in the oxidizer increases or the strain rate decreases. The effects of the oxygen content can be explained with temperature and molar fractions of the main pyrolysis products. Table 2 shows the maximum temperature, soot particle number density and molar fractions of C_2H_2, C_6H_6 and C_6H_5 with various oxygen contents in the oxidizer, and Figure 8 shows the temperature profiles using several oxygen contents in the oxidizer. In Figure 8, higher temperature is measured with higher oxygen content in the oxidizer. The breakdown paths of the fuel are

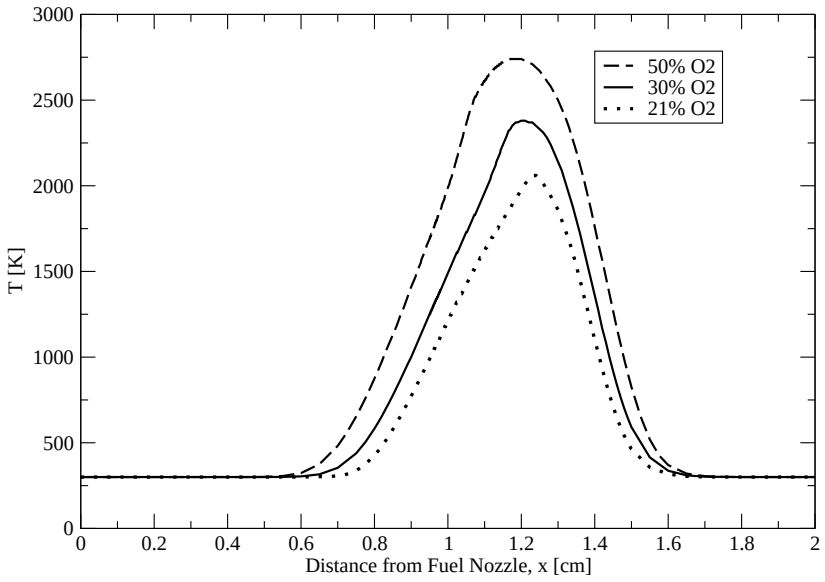

Figure 8: Temperature profiles for various oxygen contents in the oxidizer. Strain rate is 20 s^{-1}.

highly related to the activation energy, and then the difference of the maximum temperature changes the molar fraction of the species. From numerical calculation the higher molar fractions of C_2H_2, C_6H_6 and C_6H_5 are calculated between the soot inception region and the SP with higher maximum temperature. These higher molar fractions of the main pyrolysis products make soot to be incepted more, and finally this results in higher soot volume fraction.

Table 3: Maximum temperatures, stagnation points, and flame locations with various strain rates

Strain rate	Maximum Temperature	Stagnation Point	Flame location
10 s^{-1}	2400 K	0.870 cm	1.200 cm
20 s^{-1}	2378 K	0.920 cm	1.200 cm
30 s^{-1}	2364 K	0.966 cm	1.210 cm

In addition to the oxygen content in the oxidizer, the strain rate also affects the soot volume fraction. Figures 9 and 10 show the temperature and molar fraction of C_6H_6 with various strain rates but same oxygen content. The maximum temperatures, SPs and flame

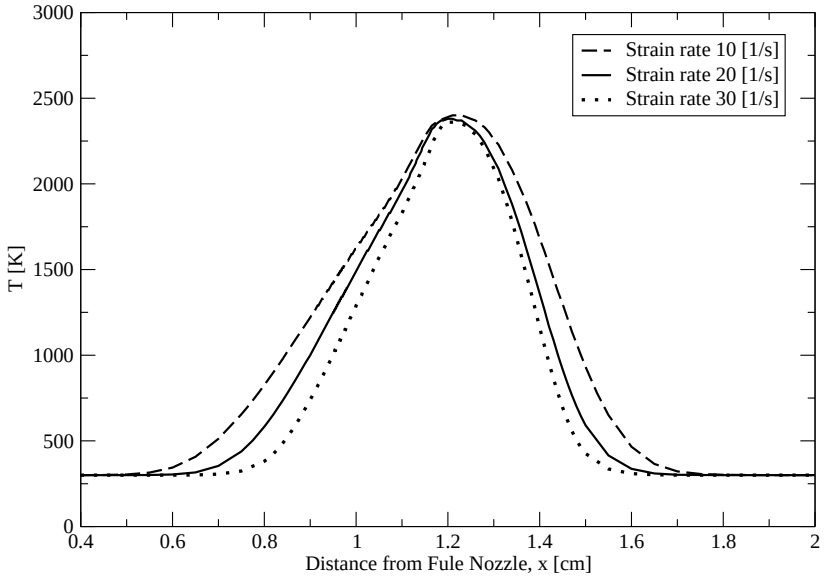

Figure 9: Temperature profiles for various strain rate. Oxidizer is composed with 30% O_2 / 70% N_2.

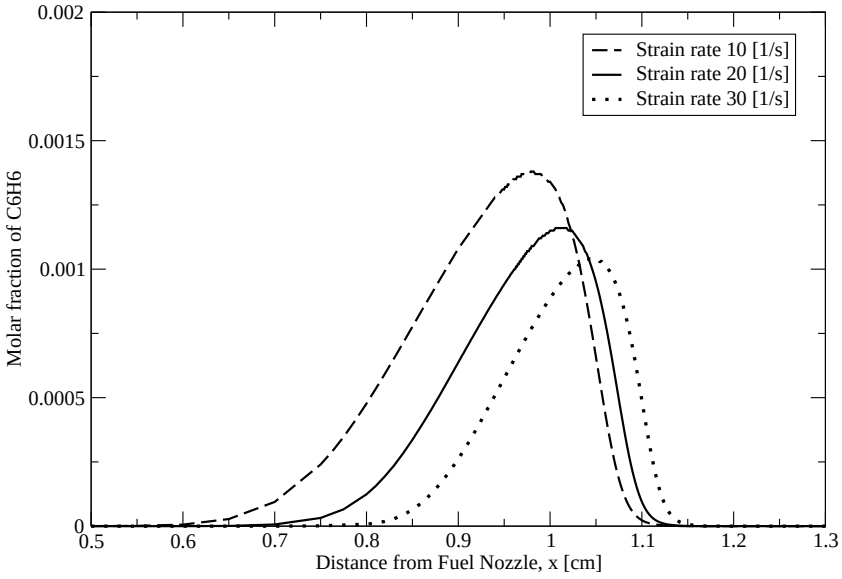

Figure 10: Profiles of C_6H_6 molar fractions for various strain rate. Oxidizer is composed with 30% O_2 / 70% N_2.

locations are shown in Table 3. In Figure 9 and Table 3, the strain rate does not affect the maximum temperature and the flame location significantly, but lower strain rate increases the residence time. Accordingly, the temperature profile becomes wider and the SPs move to the side of the fuel nozzle. When the temperature profiles are wider with the lower strain rate, the fuel that is diffused toward the high temperature region is pyrolyzed earlier. The profile of main pyrolysis product, C_6H_6, in Figure 10 shows the effect of strain rate. Therefore, when the strain rate becomes lower, the pyrolysis product, C_6H_6, is formed earlier, and finally soot inception and soot surface growth occur vigorously in the wider region between the flame and SP.

5.2 Validation of Simplified Soot Model using Acetylene with Wang et al.'s detailed reaction mechanism in Ethylene Flame

As the second validation case the fuel (ethylene) and oxidizer (air) are supplied from two opposing nozzles with a distance of 1 cm, and the initial temperatures of both sides are 300 K. The nozzle velocities are chosen such that the calculated velocity profile aligns well with the experimental results. The numerical data are compared to the experimental and calculated results provided by Wang et al. [39].

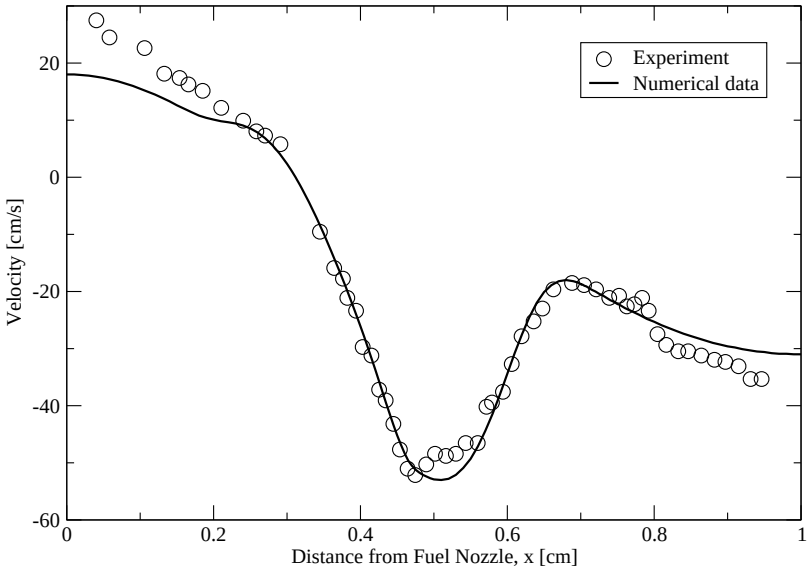

Figure 11: Experimental (symbols) and numerical (line) velocity profiles for ethylene/air flame.

Figure 11 shows the experimental and numerical velocities. In both nozzle exits, the numerical velocities are less than the experimental velocities since shield gas effect and other differences makes it difficult to properly capture the experimental conditions in a 1D setup. Law et al. [15] have shown that with the adjusted nozzle exit velocities, the calculated velocity and temperature profiles align well with the measured profiles. This approach is taken here as well.

Comparison of the numerical soot volume fraction with Wang et al. [39] 's experimental and calculated results are shown in Figure 12. They combined the numerical formulation

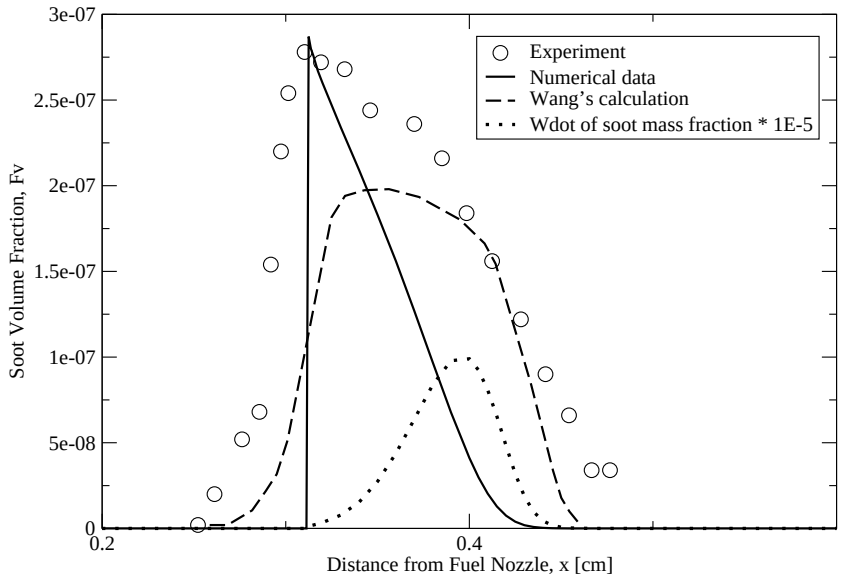

Figure 12: Numerical (solid line), Wang et al. [39] 's experimental (symbols) and calculated (dotted line) soot volume fraction profiles for ethylene-air flame.

of the counterflow problem [28, 25] with a soot model used method of moments based on the particle size distribution function (PDF) [9]. Their soot model used the gas-phase reaction chemistry primarily from an updated reaction mechanism of acetylene and ethylene oxidation and PAH formation in flames [40], and soot particle transport via diffusion, thermophoresis, and convection is considered. In the current numerical work, the stagnation point is 0.3113 cm, and the maximum soot volume fraction is 2.87E-7 at a point right after the stagnation point, $x = 0.3125$ cm. The experimental maximum soot volume fraction is 2.78E-7 at $x = 0.3103$ cm and the calculated value is 2.0E-7 at $x = 0.3562$ cm. The difference between the experimental and numerical maximum soot volume fraction is around 3 %, and the current prediction is more accurate than Wang et al [39] 's result. However, the soot volume fraction is under-predicted elsewhere because the present work ignores the soot diffusion effect.

Figures 13–14 show that the soot particle number density and the soot particle diameter. The present calculation under-predicts the soot particle number density and over-predicts the soot particle diameter compared with the Wang et al. [39] 's calculation. The profiles

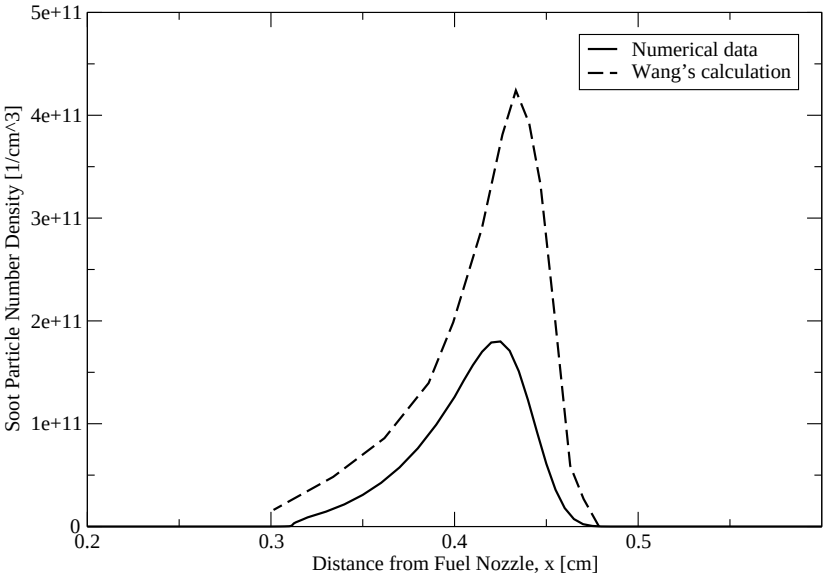

Figure 13: Present numerical (solid line) and Wang et al. [39] 's calculated (dotted line) soot particle number density profiles for ethylene/air flame.

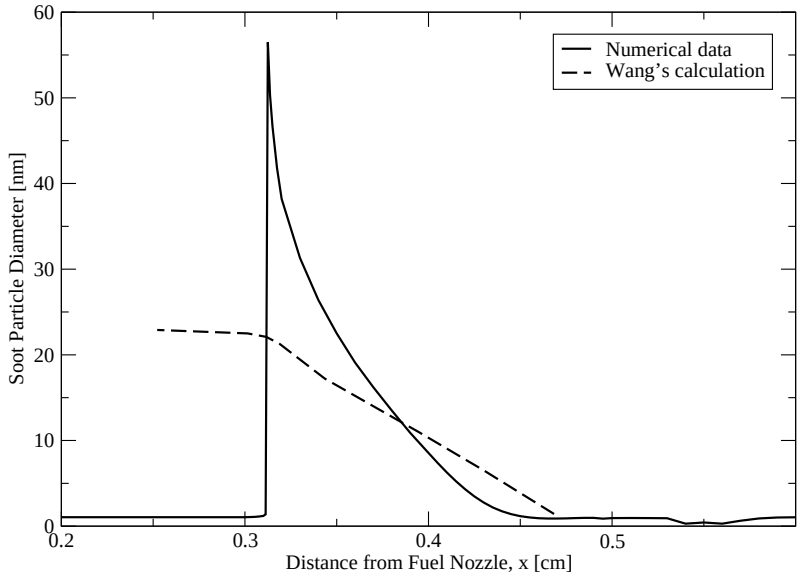

Figure 14: Present numerical (solid line) and Wang et al. [39] 's calculated (dotted line) soot particle diameter profiles for ethylene/air flame.

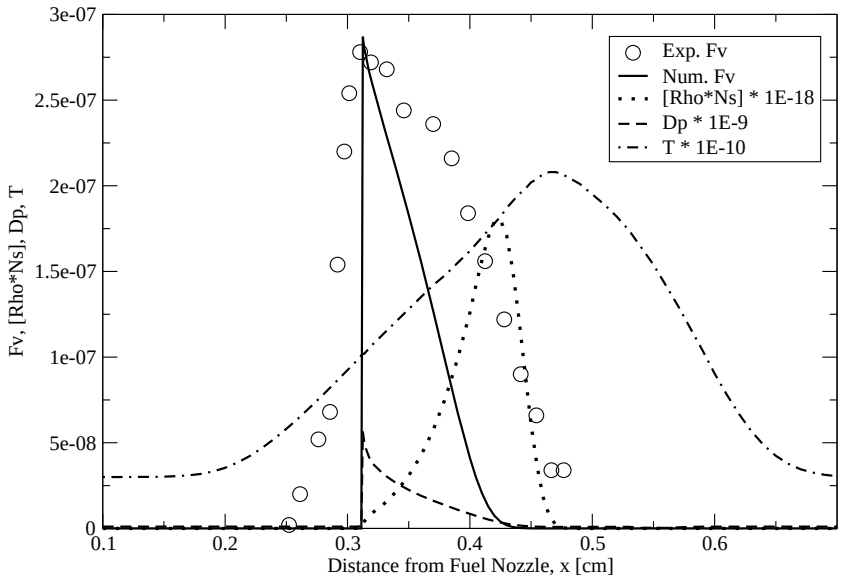

Figure 15: Profiles of soot volume fraction, soot particle number density, soot particle diameter and temperature for ethylene/air flame.

of the soot volume fraction, soot particle number density, soot particle diameter and temperature are shown in Figure 15. The soot particle number density $[\rho N_s]$ increases between $x = 0.470\ cm$ which is just before the location of the maximum temperature, 2077 K, and around $x = 0.42\ cm$ by the soot inception. It then decreases from $x = 0.42\ cm$ to the stagnation point with increasing the soot particle diameter by the soot surface growth and agglomeration. With increase in the soot particle diameter, the soot volume fraction also increases. These characteristics of the soot production and destruction are similar to the results reported earlier (Figure 6) for methane-air mechanism.

5.3 Comparison of Beltrame et al.'s Detailed Reaction Mechanism and 12-step, 16-species Reduced Reaction Mechanism in Methane Flame

In section 5.1, it was shown that the simplified soot model which uses benzene as main pyrolysis product based on the Beltrame's detailed reaction mechanism provides results that are consistent with experimental data at certain strain rates and oxygen contents in the methane flame. However, as mentioned before, the detailed reaction mechanism is not practical to model real combustor systems because of computation costs. Therefore, it is necessary to determine how soot is predicted when a reduced reaction mechanism is employed. Sung et al. [32] already proved that the reduced reaction mechanism can provide accurate results for the major species. The goal here is to determine whether the simplified soot model that uses acetylene, which is a minor species for a non sooting methane-/air flame, as a main pyrolysis product to calculate the soot volume fraction is accurate.

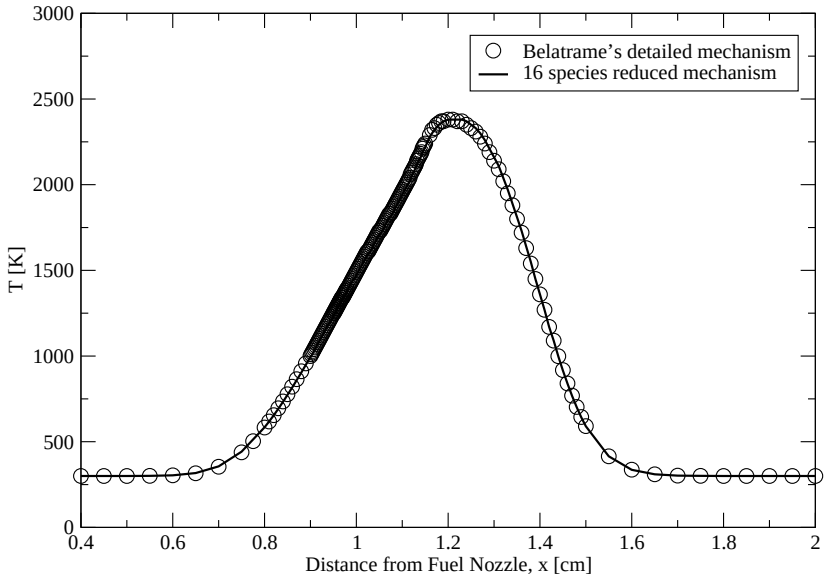

Figure 16: Temperature profiles using reduced(solid line) and detailed (symbol) reaction mechanism for the methane / 30% oxygen flame. Strain rate is 20 s^{-1}.

Figures 16 – 19 compare the profiles of temperature, flow velocity, density and all key species based on the Beltrame's detail reaction mechanism and the 12-step, 16-species reduced reaction mechanism with exactly the same initial and boundary conditions: the fuel

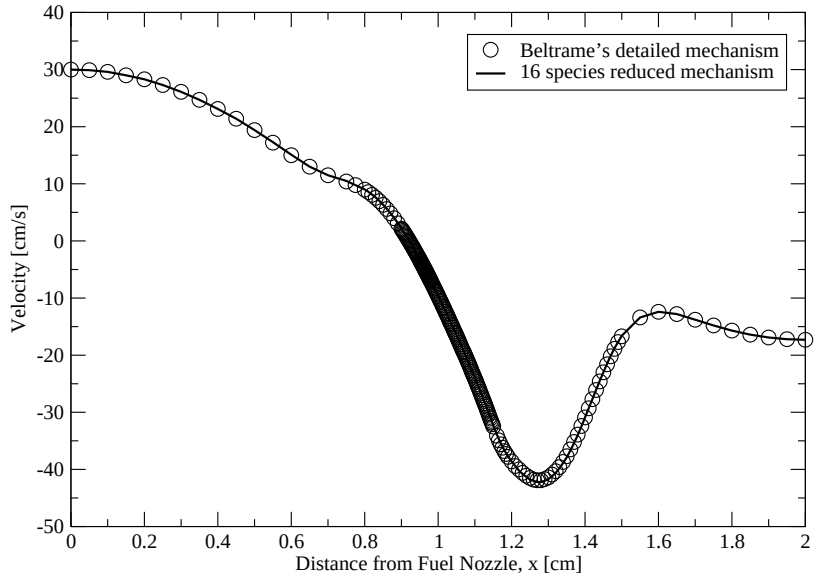

Figure 17: Flow velocity profiles using reduced (solid line) and detailed (symbol) reaction mechanism for the methane / 30% oxygen flame. Strain rate is 20 s^{-1}.

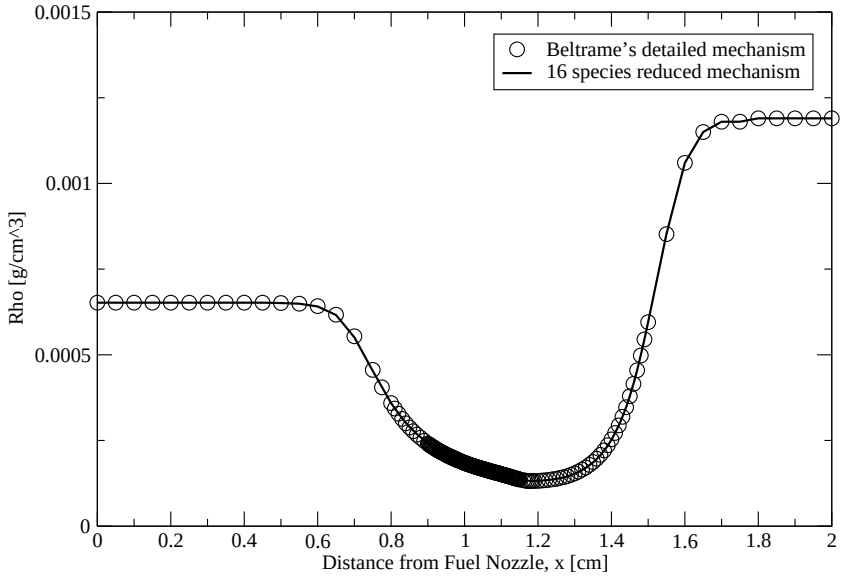

Figure 18: Density profiles using reduced (solid line) and detailed (symbols) reaction mechanism for the methane / 30% oxygen flame. Strain rate is 20 s^{-1}.

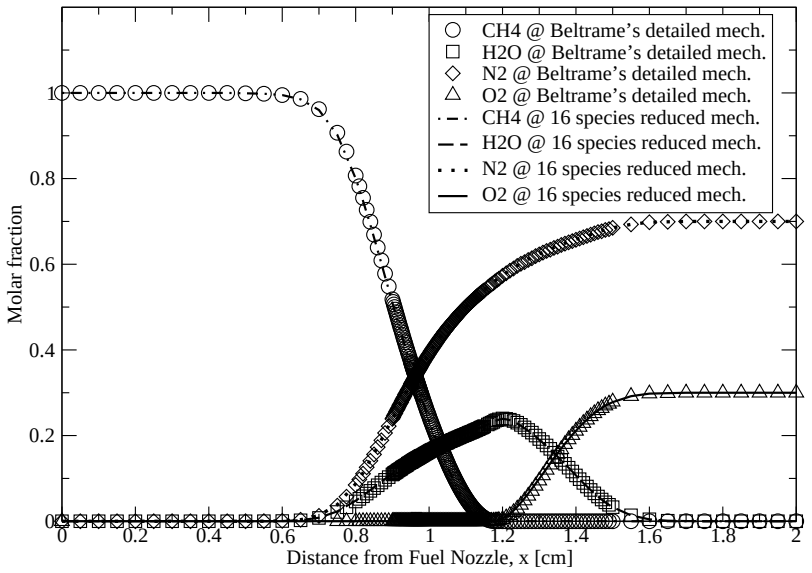

Figure 19: Major species profiles using reduced (lines) and detailed (symbols) reaction mechanism for the methane / 30% oxygen flame. Strain rate is 20 s^{-1}.

(methane) and oxidizer (oxygen/nitrogen mixture) are supplied from two opposing nozzles with a distance of 2 cm. The initial temperatures of both sides are $300K$, and the strain rate is 20 s^{-1}. The nozzle velocities are calculated based on the strain rate. The temperature, density, velocity and the major species predicted by the 12-step, 16-species reduced reaction mechanism agree very well with the Beltrame's detailed reaction mechanism predictions.

Figures 20 – 22 compare the profiles of selected minor species such as C_2H_2, CH_3, C_2H_4,C_2H_6, O, and OH. It can be seen that the minor species are over-predicted by the 12-step, 16-species reduced reaction mechanism. As mentioned above, the simplified soot model based on the 12-step, 16-species reduced reaction mechanism uses acetylene, C_2H_2, as a main pyrolysis product. Therefore, the over-prediction of acetylene in Figure 20 makes the simplified soot model also over-predict the soot volume fraction as is shown in Figure 23. In Table A4 of the Appendix, the peak values of soot volume fraction using reduced reaction mechanism compare with the experimental results and numerical calculation using the detailed reaction mechanism at the oxygen contents of 21%, 30%, and 50% with various strain rates. These over-predictions of the soot volume fraction in Figure 23 and Table A4 implies that the prediction of the minor species with the 12-step, 16-species reduced

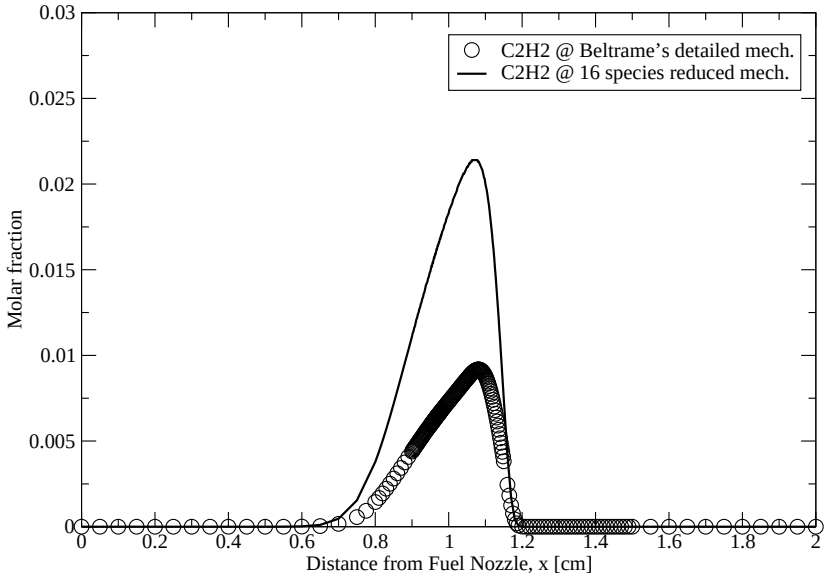

Figure 20: C_2H_2 profiles using reduced (solid line) and detailed (symbol) reaction mechanism for the methane / 30% oxygen flame. Strain rate is 20 s^{-1}.

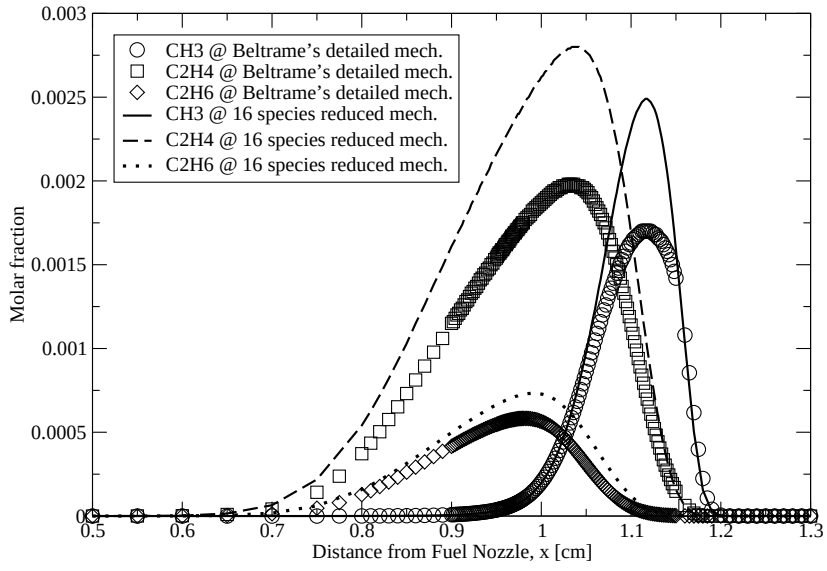

Figure 21: CH_3, C_2H_4, C_2H_6 profiles using reduced (solid line) and detailed (symbol) reaction mechanism for the methane / 30% oxygen flame. Strain rate is 20 s^{-1}.

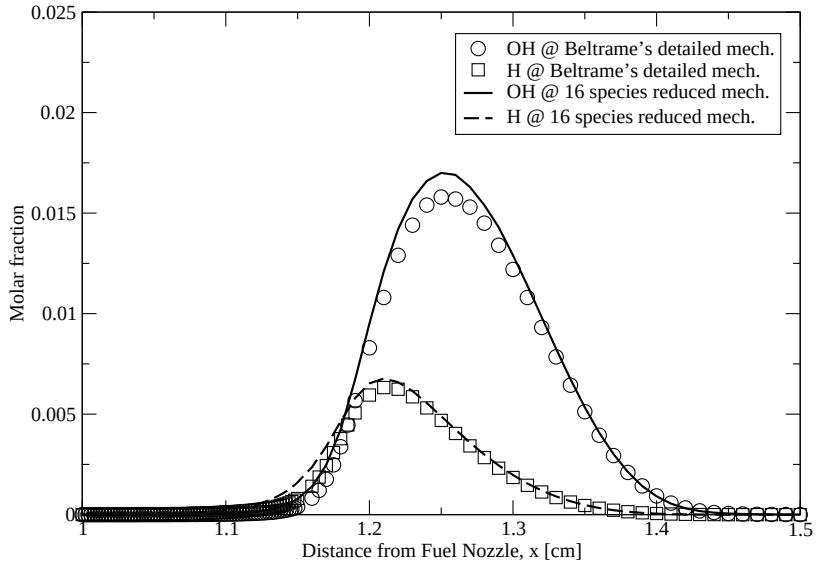

Figure 22: OH, H profiles using reduced (solid line) and detailed (symbol) reaction mechanism for the methane / 30% oxygen flame. Strain rate is 20 s^{-1}.

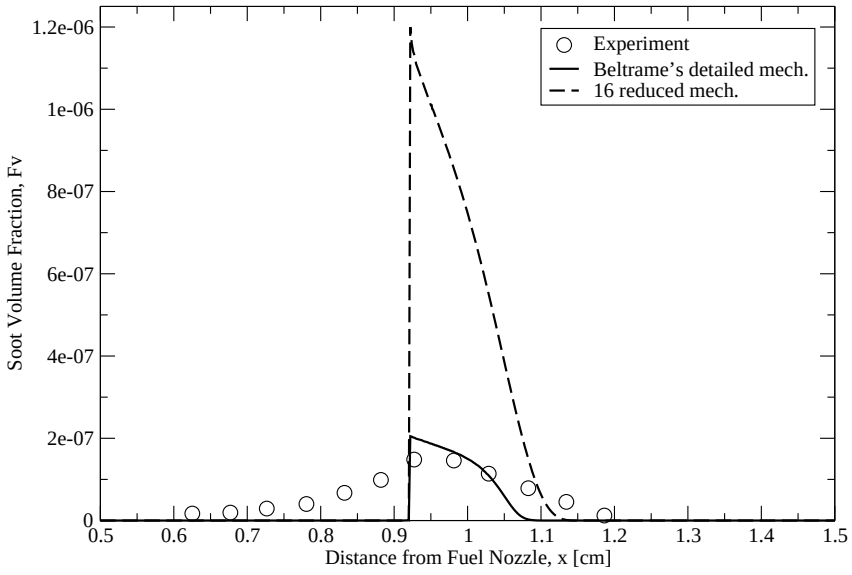

Figure 23: Profile of soot volume fraction based on reduced (solid line) and detailed (dotted line) reaction mechanism with experiment for the methane / 30% oxygen flame. Strain rate is 20 s^{-1}.

reaction mechanism needs to be improved to get more accurate soot prediction.

The over-predicted profile of the soot volume fraction in Figure 23 also shows that the inception point is shifted by approximately 0.1 cm in respect to the soot volume fraction using the detailed reaction mechanism. However, if the profile of the over-predicted soot volume fraction is shrunk to match to the profile of the soot volume fraction using the detailed reaction mechanism, the inception points coincide.

5.4 Comparison of Wang et al.'s Detailed Reaction Mechanism and 20-species Reduced Reaction Mechanism in Ethylene Flame

Here, the results from the Wang et al. [39] 's detailed reaction mechanism are compared with the results using a 20-species reduced reaction mechanism [31]. The same simplified soot model which uses acetylene as the main pyrolysis product is employed for both. The initial and boundary conditions of both numerical calculations are exactly same: the fuel (ethylene) and oxidizer (air) are supplied from two opposing nozzles with a distance of 1 cm. The initial temperatures of the fuel and oxidizer are 300 K.

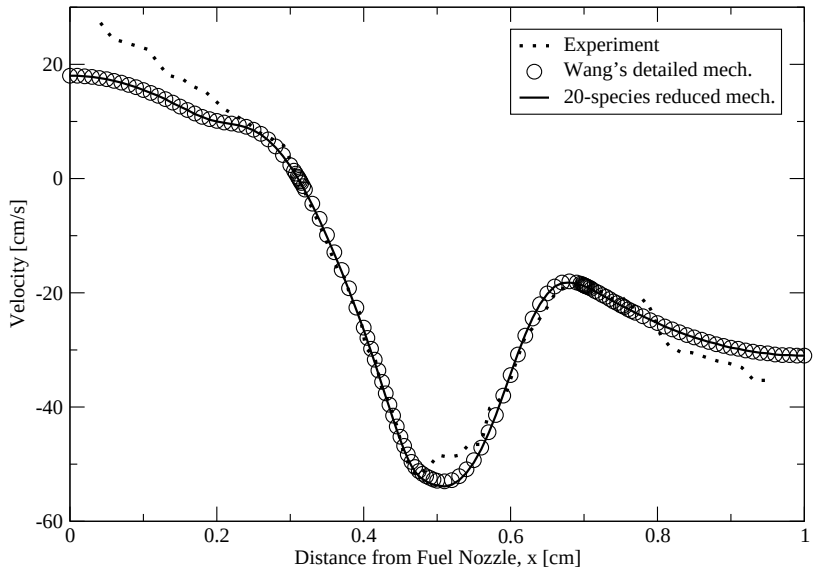

Figure 24: Velocity profiles using reduced (solid line) and detailed (symbol) reaction mechanism with experimental velocity (dotted line) for the ethylene/air flame.

Velocity, temperature and major species profiles are compared in Figs. 24 – 27. Because of lack of experimental results, Figs. 25 – 27 show only the numerical results. Similar to Chapter 5.3, the profiles of velocity, temperature and major species which are calculated by the simplified soot model based on the 20-species reduced reaction mechanism coincide with the results based on Wang et al. [39] 's detailed reaction mechanism. However, some minor species, such as C_2H_2, CH_3 and CH_4, are over-predicted as shown in Figs. 28 – 29, and these differences affect to the soot volume fraction, particle number density and

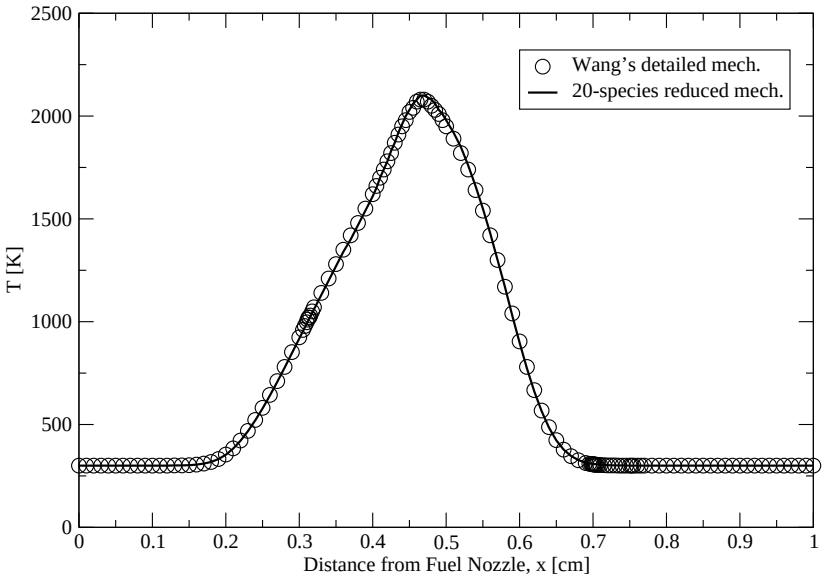

Figure 25: Temperature profiles using reduced (line) and detailed (symbol) reaction mechanism for the ethylene/air flame.

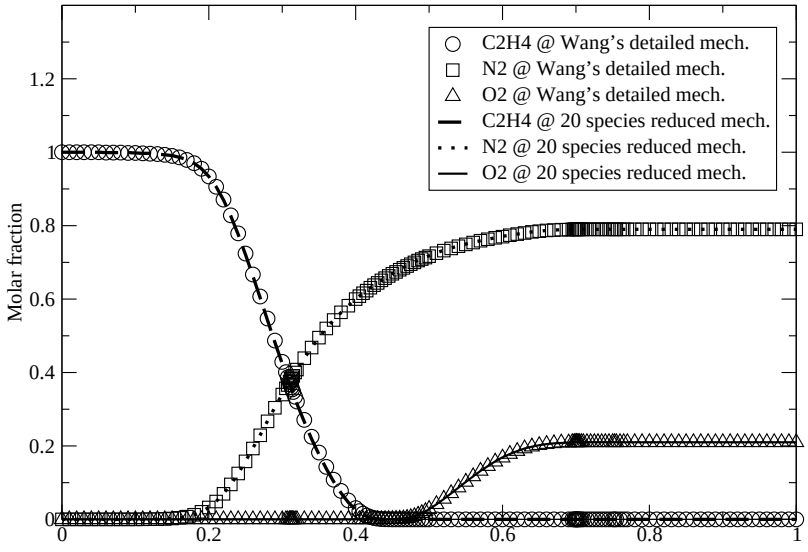

Figure 26: Major species profiles using reduced (line) and detailed (symbol) reaction mechanism for the ethylene/air flame.

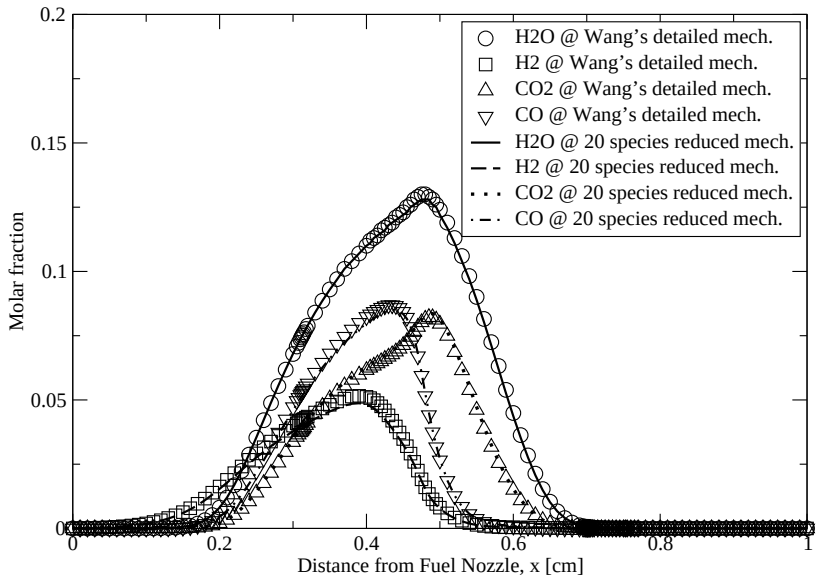

Figure 27: Major species profiles using reduced (line) and detailed (symbol) reaction mechanism for the ethylene/air flame.

particle diameter.

Finally, Figs. 30 – 32 compare the two numerical results based on Wang et al. [39] 's detailed reaction mechanism and 20-species reduced mechanism with the earlier experimental and numerical data [39]. Similar to Figure 23, over-predicted acetylene in Figure 28 causes the soot volume fraction, particle number density and particle diameter based on the 20-species reduced mechanism to be over-predicted when compared to the Wang et al. [39] 's detailed reaction mechanism predictions. However, the soot inception location and location of maximum are very similar.

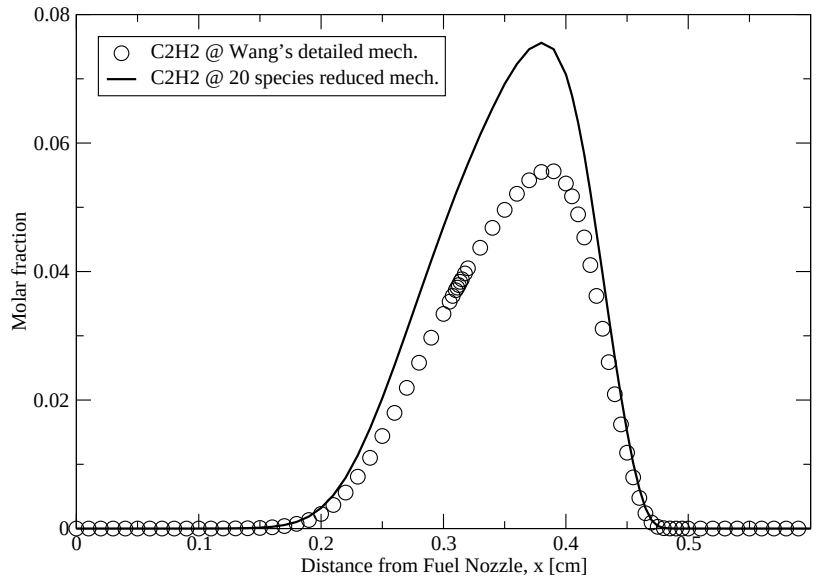

Figure 28: Acetylene profiles using reduced (line) and detailed (symbol) reaction mechanism for the ethylene/air flame.

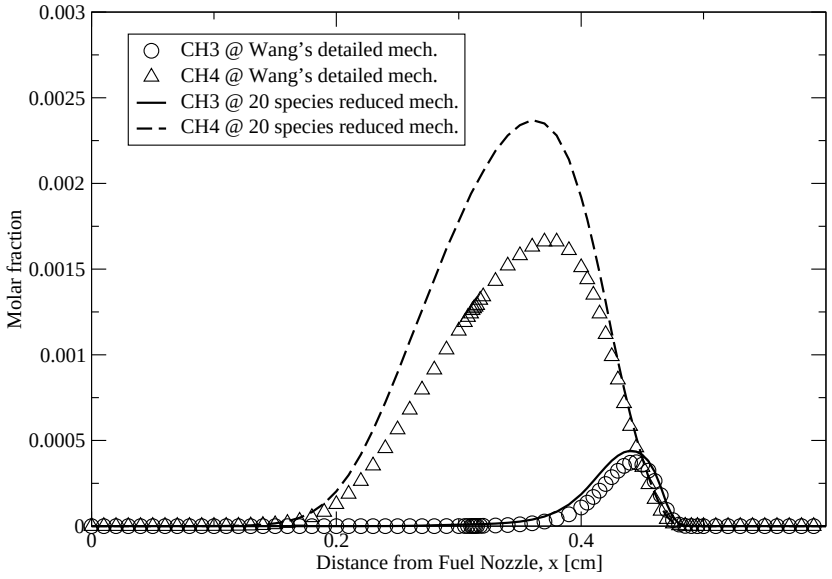

Figure 29: Profiles of CH3 & CH4 using reduced (line) and detailed (symbol) reaction mechanism for the ethylene/air flame.

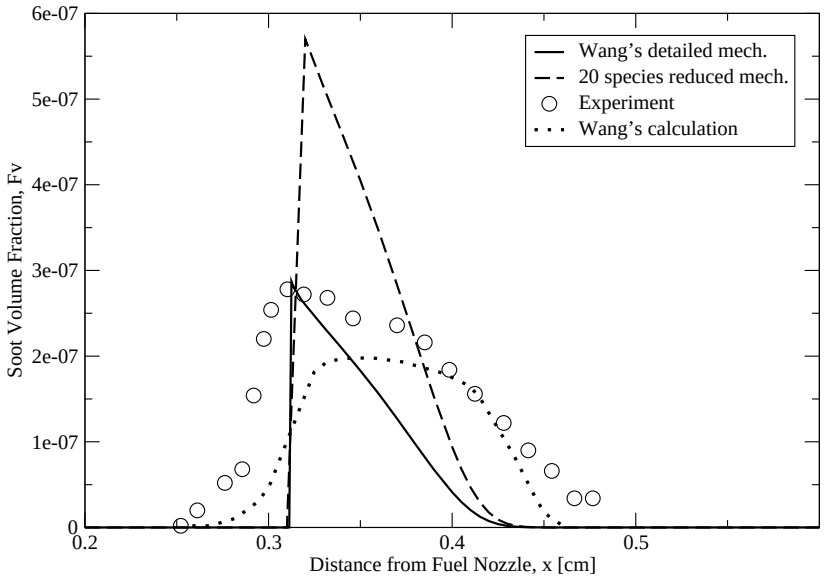

Figure 30: Profiles of the soot volume fraction using detailed (solid line) and reduced (dotted line) reaction mechanism with experiment (symbols) and calculation (dots) by Wang et al. for the ethylene/air flame.

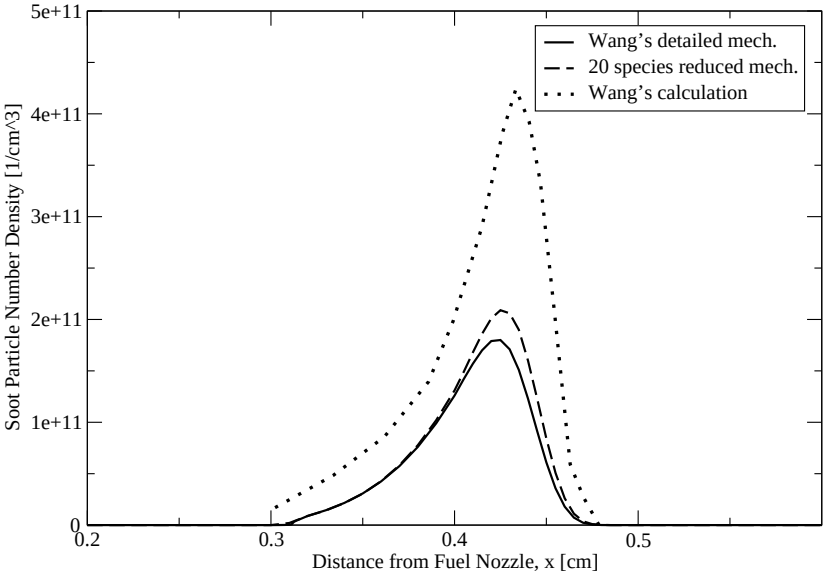

Figure 31: Profiles of the soot particle number density using detailed (solid line) and reduced (dotted line) reaction mechanism with Wang et al.'s calculation (dots) for the ethylene/air flame.

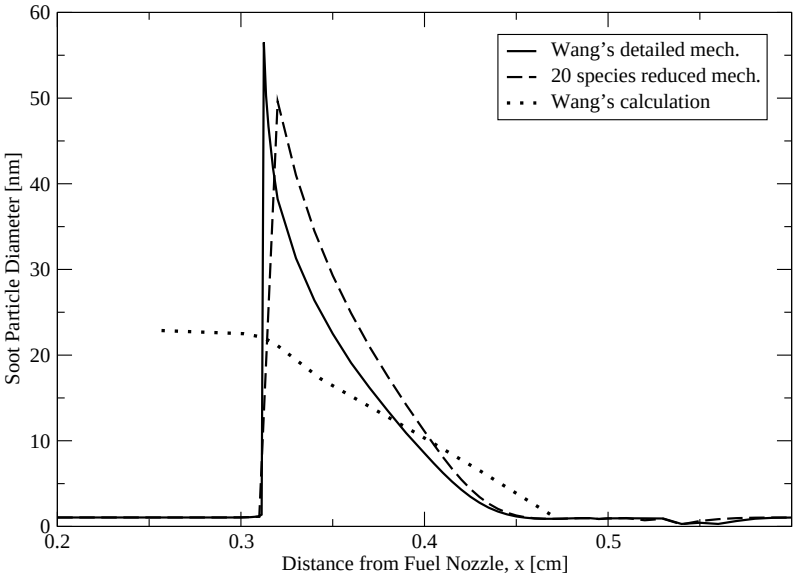

Figure 32: Profiles of the soot particle diameter using detailed (solid line) and reduced (dotted line) reaction mechanism with Wang et al.'s calculation (dots) for the ethylene/air flame.

5.5 Modification of the 12-step, 16-species reduced reaction mechanism

Since both reduced reaction mechanism in Chapters 5.3 – 5.4 over-predict or under-predict some minor species and soot related properties, such as volume fraction, particle number density and particle diameter, they need to be improved to get better accurate soot prediction. To predict the soot volume fraction correctly within the reduced reaction mechanisms, the coefficients of the reduced reaction mechanisms are modified to match the molar fraction of the minor species to the results based on the detailed reaction mechanism. These modifications are done such that all the physical properties and the molar fraction of the major species are not affected. Table A3 of the Appendix shows the modified rate coefficients.

Figures 33 and 34 show the temperature and the major species profiles, respectively. The simplified soot model using a modified 16-species reduced mechanism compares well with the model based on Beltrame et al [1] 's detailed mechanism and the original 16-species reduced mechanism.

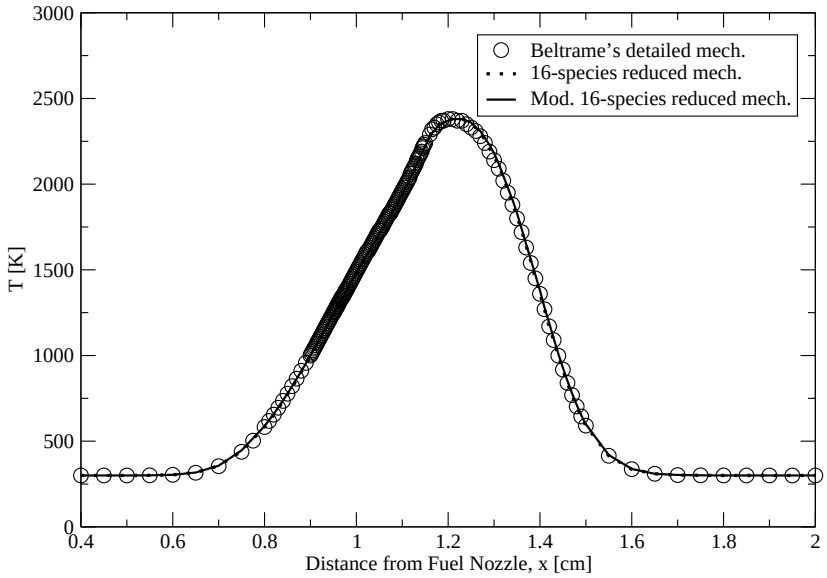

Figure 33: Temperature profiles using modified reduced (solid line) reaction mechanism with reduced (dots) and detailed (symbols) reaction mechanism for the methane / 30% oxygen flame. Strain rate is 20 s^{-1}.

However, even though the modified 16-species reduced reaction mechanism does not

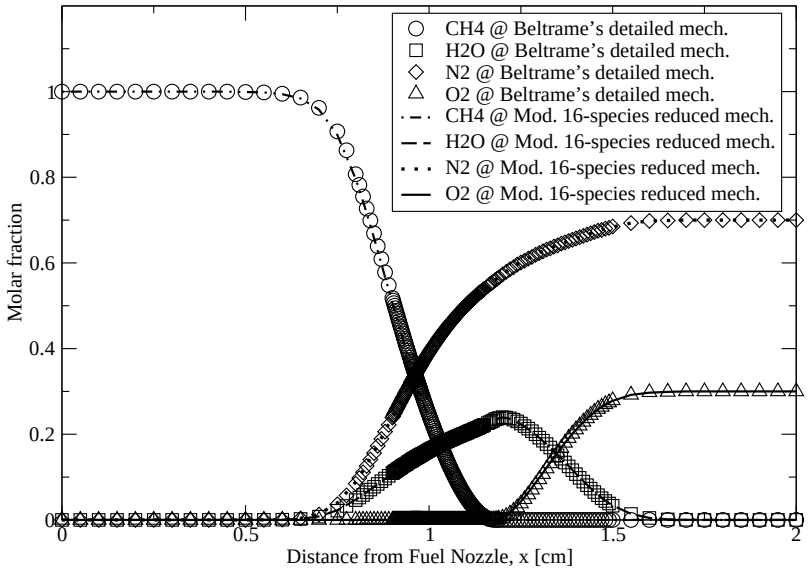

Figure 34: Major species profiles using modified reduced (lines) and detailed (symbols) reaction mechanism for the methane / 30% oxygen flame. Strain rate is 20 s^{-1}.

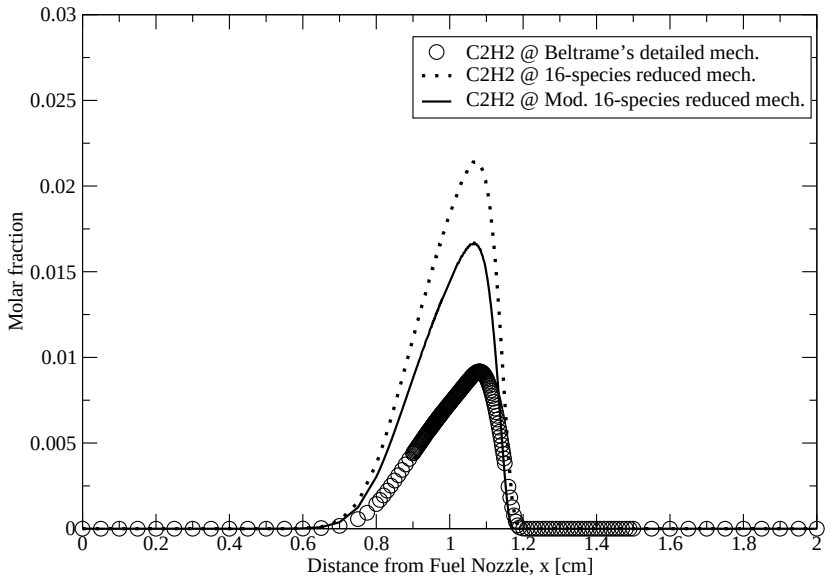

Figure 35: C_2H_2 profiles using modified reduced (solid line) reaction mechanism with reduced (dots) and detailed (symbol) reaction mechanism for the methane / 30% oxygen flame. Strain rate is 20 s^{-1}.

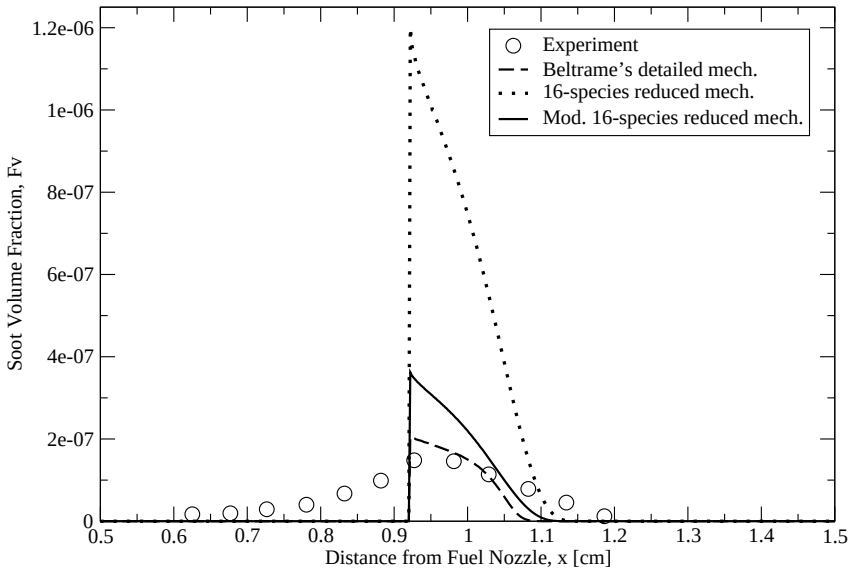

Figure 36: Profiles of the soot volume fraction based on modified reduced (solid line), detailed(dots) and reduced (dotted line) reaction mechanism with experiment (symbols) for the ethylene-air flame.

affect the physical properties and major species, it has a drastic influence on some minor species. Figure 35 shows molar fractions of C_2H_2 with various reaction mechanisms. The simplified soot model based on the modified 16-species reduced reaction mechanism reduces the molar fraction of C_2H_2. This cause the soot volume fraction decreases, too. The profiles of the soot volume fraction are shown in Figure 36. The maximum soot volume fraction with the modified 16-species reduced mechanism is still higher than experimental results, but the discrepancy of the peak values between the detailed reaction mechanism and the reduced reaction mechanism decreases. Table A4 of the Appendix compares the peak values of soot volume fraction at the oxygen contents of 21%, 30%, and 50% with various strain rates. The table shows that the modified reduced reaction mechanism results in a smaller soot volume fraction than the reduced reaction mechanism. Since the modified reduced reaction mechanism is tuned for the oxygen content of 30% and for a strain rate of 20 $[s^-1]$, the soot volume fractions with different oxygen contents and strain rates can be lower than the experimental results.

CHAPTER VI

CONCLUSION

The soot volume fractions which are calculated using a simplified soot model based on two different detailed reaction mechanisms are consistent with the experimental results, and the profiles of the other physical properties and the major species are reasonable. However, the detailed reaction mechanisms are not computationally practical to model real complex systems, because reactions and species are too large: Beltrame et al. [1] 's detailed reaction mechanism consists of 361-reactions and 61-species, and Wang et al. [39] includes 527-reactions and 99-species.

The reduced reaction mechanisms that was proposed by Sung et al. [32] are the 12-step, 16-species process for methane flame and the 20-species process for ethylene flame. The reduced reaction mechanisms cut down the computation time and results show that the profiles of the physical properties and the major species are consistent with the results based on the detailed reaction mechanisms.

The simplified soot model uses acetylene as the primary pyrolysis species. Results show that acetylene is over-predicted by the reduced reaction mechanisms and this impacts also the soot prediction. Therefore it is clear that the minor species such as acetylene, ethylene and ethane, have to predict more accuretely within the reduced mechanism. This is an issue for further research.

When Sung et al. [32] suggested the reduced reaction mechanisms used in the present work, the reduced reaction mechanisms was designed specifically for methane or ethylene oxidation only. The mechanisms calculate a few species related to the oxidation process, but apply steady-state approximation to the other species. These issues have to addressed explicitly so that the reduced mechanism can also include more accurate prediction of hydrocarbon-species. This is confirmed here by modifying the mechanism to improve the prediction of acetylene and then using this mechanism with the soot model. Results show

that soot prediction can be improved by improving the predictions of the key minor species in the reduced mechanism.

In summary, this study have shown that a reduced mechanism coupled with a simplified soot model can be used for soot prediction in a computationally efficient manner. Although there is an over-prediction of soot volume fraction, the location of peak and the overall trends are well reproduced. This study has also identified the key minor hydrocarbon-species in the reduced mechanism that need to be improved for better soot prediction. This remains to be demonstrated.

CHAPTER VII

APPENDIX

Table A1: Extended reaction mechanism for benzene and soot model. Rate cefficient in the form $K_f = AT^{\beta}exp(-E/RT)$ (units are moles, cubic centimeters, seconds, Kelvins and calories per mole)

	Reaction	A	β	E
280	$C_3H_3 + H \Rightarrow C_3H2 + H_2$	5.00E+13	0	3000
281	$C_3H_3 + OH \Rightarrow C_3H_2 + H_2O$	1.00E+13	0	0
282	$CH + C_2H_2 \Rightarrow C_3H_2 + H$	1.00E+14	0	0
283	$C_3H_2 + O_2 = HCCO + CO + H$	1.00E+14	0	2999.3
284	$C_3H_2 + OH = C_2H_2 + HCO$	5.00E+13	0	0
285	$C_3H_2 + O_2 = HCO + HCCO$	1.00E+13	0	0
286	$CH_2 + C_2H_2 = H + C_3H_3$	1.20E+13	0	6618.6
287	$CH_2(S) + C_2H_2 = C_3H_3 + H$	1.80E+14	0	0
288	$HCCO + C_2H_2 = C_3H_3 + CO$	1.00E+11	0	2999.3
289	$C_3H_4 + M = C_3H_3 + H + _M$	2.00E=18	0	79,982.6
	H_2O	Enhanced	by	1.60E+01
	CO_2	Enhanced	by	3.75E+00
	CO	Enhanced	by	1.87E+00
	H_2	Enhanced	by	2.50E+00
	CH_4	Enhanced	by	3.00E+00
	C_2H_4	Enhanced	by	1.60E+01
290	$C_3H_4 + O_2 = C_3H_3 + HO_2$	4.00E+13	0	61,486.7
291	$C_3H_4 + OH = C_3H_3 + H_2O$	2.00E+07	2	999.8
292	$C_3H_4 + H = C_3H_3 + H_2$	2.00E+07	2	2998.9
293	$C_3H_4 + CH_3 = C_3H_3 + CH_4$	2.00E+11	0	7698.3
294	$PC_3H_4 + M = C_3H_3 + H + M$	4.70E+18	0	79,982.6

Table A1: Continued

	Reaction	A	β	E
295	$PC_3H_4 + O2 = C_3H_3 + HO_2$	5.00E+12	0	50,988.9
296	$PC_3H_4 + OH = C_3H_3 + H_2O$	8.00E+07	2	1000.8
297	$PC_3H_4 + H = C_3H_3 + H_2$	1.00E+07	2	5000
298	$PC_3H_4 + CH_3 = C_3H_3 + CH_4$	1.50E+00	5	5598.8
299	$PC_3H_4 + C_2H_3 = C_3H_3 + C_2H_4$	1.00E+12	0	7698.3
300	$C_3H_3 + O \Rightarrow C_2H + HCO + H$	1.39E+14	0	0
301	$C_3H_3 + O \Rightarrow C_2H_2 + CO + H$	1.40E+14	0	0
302	$C_3H_3 + O_2 = CH_2CO + HCO$	3.01E+10	0	2869.4
303	$C_3H_3 + CH = NC_4H_3 + H$	7.00E+13	0	0
304	$C_3H_3 + CH_2 = C_4H_4 + H$	4.00E+13	0	0
305	$2C_4H_4 \Rightarrow C_6H_5 + H$	2.00E+12	0	0
306	$C_3H_3 + O \Rightarrow C_2H_3 + CO$	3.80E+13	0	0
307	$C_3H_3 + O = CH_2O + C_2H$	2.00E+13	0	0
308	$C_3H_3 + O_2 \Rightarrow HCCO + CH_2O$	6.00E+12	0	0
309	$C_3H_3 + CH_3 = C_2H_5 + C_2H$	1.00E+13	0	37,491.9
310	$C_3H_4 + C_2H = C_3H_3 + C_2H_2$	1.00E+13	0	0
311	$PC_3H_4 + C_2H = C_3H_3 + C_2H_2$	1.00E+13	0	0
312	$2C_3H_3 \Rightarrow C_6H_6$	3.00E+11	0	0
313	$C_3H_3 + C_3H_4 \Rightarrow C_6H_6 + H$	1.40E+12	0	9997.8
314	$C_3H_3 + N = HCN + C_2H_2$	1.00E+13	0	0
315	$C_2H_3 + CH_2 = C_3H_4 + H$	3.00E+13	0	0
316	$C_2H_2 + CH_3 = C_3H_4 + H$	6.74E+19	-2.1	31,584.1
317	$C_3H_4 = PC_3H_4$	1.20E+15	0	92,380
318	$C_3H_4 + OH = CH_2CO + CH_3$	3.12E+12	0	-396.9
319	$C_3H_4 + O = C_2H_3 + HCO$	1.10E-02	4.6	-4242.1
320	$C_3H_4CY = C_3H_4$	1.51E+14	0	50,389.1
321	$CH_2 + C_2H_2 = C_3H_4$	1.20E+13	0	6618.6
322	$C_3H_4 + OH = CH_2O + C_2H_3$	1.70E+12	0	-299.9
323	$C_3H_4 + OH = HCO + C_2H_4$	1.70E+12	0	-299.9
324	$C_3H_4 + O = CH_2O + C_2H_2$	1.00E+12	0	0
325	$C_3H_4 + O \Rightarrow CO + C_2H_4$	7.80E+12	0	1599.7
326	$C_3H_4 + HO_2 \Rightarrow CH_2CO + CH_2 + OH$	8.00E+12	0	18,995.9
327	$C_3H_4CY = PC_3H_4$	7.08E+13	0	43,690.5
328	$PC_3H_4 + O_2 \Rightarrow HCCO + OH + CH_2$	2.00E+08	1.5	30,093.5
329	$PC_3H_4 + HO_2 \Rightarrow C2H4 + CO + OH$	3.00E+12	0	18,995.9
330	$PC_3H_4 + OH = CH_2CO + CH_3$	5.00E-04	4.5	-999.8

Table A1: Continued

	Reaction	A	β	E
331	$PC_3H_4 + O = CH_2CO + CH_2$	6.40E+12	0	2009.6
332	$PC_3H_4 + O = C_2H_3 + HCO$	3.20E+12	0	2009.6
333	$PC_3H_4 + O = HCCO + CH_3$	6.30E+12	0	2009.6
334	$PC_3H_4 + O \Rightarrow HCCO + CH_2 + H$	3.20E+11	0	2009.6
335	$PC_3H_4 + H = C_2H_2 + CH_3$	1.30E+05	2.5	1000
336	$PC_3H_4 = C_2H + CH_3$	4.20E+16	0	99,978.3
337	$C_4H_4 + OH = NC_4H_3 + H_2O$	7.50E+06	2	4998.9
338	$C_4H_4 + H = NC_4H_3 + H_2$	2.00E+07	2	14,996.7
339	$NC_4H_3 + C_2H_2 = C_6H_5$	2.80E+03	2.9	1399.7
340	$C_3H_3 + CH = IC_4H_3 + H$	7.00E+13	0	0
341	$C_3H_2 + CH_2 = IC_4H_3 + H$	3.00E+13	0	0
342	$C_4H_4 + OH = IC_4H_3 + H_2O$	1.00E+07	2	2000
343	$IC_4H_3 + CH_2 = C_3H_4 + C_2H$	2.00E+13	0	0
344	$IC_4H_3 + O_2 = CH_2CO + HCCO$	1.00E+12	0	0
345	$IC_4H_3 + O = CH_2CO + C_2H$	2.00E+13	0	0
346	$C_2H_2 + C_2H_2 = IC_4H_3 + H$	2.30E+12	0	64,060
347	$NC_4H_3 + H = IC_4H_3 + H$	1.0-0E+14	0	0
348	$C_2H_3 + C_2H_2 = C_4H_4 + H$	2.00E+12	0	4998.9
349	$NC_4H_5 + OH = C_4H_4 + H_2O$	2.00E+07	2	999.8
350	$NC_4H_5 + H = C_4H_4 + H_2$	3.00E+07	2	999.8
351	$IC_4H_5 = C_4H_4 + H$	2.00E+15	0	44,990.2
352	$NC_4H_5 = C_4H_4 + H$	1.60E+14	0	41,391
353	$IC_4H_5 + H = C_4H_4 + H_2$	3.00E+07	2	999.8
354	$C_2H_2 + NC_4H_5 = C_6H_6 + H$	2.80E+03	2.9	1400
355	$NC_4H_5 + H = IC_4H_5 + H$	1.00E+14	0	0
356	$C_2H_2 + C_2H_3 = NC_4H_5$	2.51E+05	1.9	2099.5
357	$2C_2H_3 = IC_4H_5 + H$	4.00E+13	0	0
358	$C_6H_6 + H = C_6H_5 + H_2$	3.00E+14	0	7200
359	$C_6H_6 + OH = C_6H_5 + H_2O$	5.31E+08	1.4	1451
360	$H + C_6H_5 = C_6H_6$	3.16E+13	0	0
361	$C_6H_6 + O = C_6H_5 + OH$	1.00E+01	3.8	1790

Table A2: Reduced Reaction Mechanism

	Reaction
1	$O_2 + 2C_O = 2CO_2$
2	$H + O_2 + CO = OH + CO_2$
3	$H_2 + O_2 + CO = H + OH + CO_2$
4	$HO_2 + CO = OH + CO_2$
5	$O_2 + H_2O_2 + CO = OH + HO_2 + CO_2$
6	$O_2 + 0.5C_2H_2 = H + CO_2$
7	$O_2 + CH_3 + CO + C_2H_4 = CH_4 + CO_2 + CH_2O + 0.5C_2H_2$
8	$O_2 + 2CH_3 = H_2 + CH_4 + CO_2$
9	$O_2 + 2CH_3 + CO = CH_4 + CO_2 + CH_2O$
10	$O_2 + CH_3 + CO = H + CO_2 + CH_2O$
11	$O_2 + CO + C_2H_6 = CH_4 + CO_2 + CH_2O$
12	$H + OH = H_2O$

Table A3: Modified & original rate coefficient of GRI-Mech 2.11 in the 12-step, 16-species reduced mechanism. Rate cefficient in the form $K_f = AT^{\beta}exp(-E/RT)$ (units are moles, cubic centimeters, seconds, Kelvins and calories per mole)

	Reaction	modified A	original A	β	E
21	$O + C_2H_2 \Leftrightarrow H + HCCO$	1.020E+08	1.020E+07	2.000	1900.00
23	$O + C_2H_2 \Leftrightarrow CO + CH_2$	1.020E+08	1.020E+07	2.000	1900.00
72	$H + C_2H_3 \Leftrightarrow H_2 + C_2H_2$	8.000E+12	3.000E+13	0	0
106	$OH + C_2H_2 \Leftrightarrow H + CH_2CO$	1.090E-03	2.180E-04	4.500	1000.00
123	$C + CH_3 \Leftrightarrow H + C_2H_2$	5.000E+11	5.000E+13	0	0
127	$CH + CH_2 \Leftrightarrow H + C_2H_2$	4.000E+11	4.000E+13	0	0
133	$CH + HCCO \Leftrightarrow CO + C_2H_2$	5.000E+11	5.000E+13	0	0
136	$2CH_2 \Leftrightarrow H_2 + C_2H_2$	3.200E+11	3.200E+13	0	0
170	$C_2H + H_2 \Leftrightarrow H + C_2H_2$	4.070E+03	4.070E+05	2.400	200.00
175	$2HCCO \Leftrightarrow 2CO + C_2H_2$	1.000E+11	1.000E+13	0	0

Table A4: Peak values of soot volume fraction as a function of oxygen content and strain rate

	Experimental results			Detailed reaction mechanism		
Strain rate $[s^{-1}]$	21%	30%	50%	21%	30%	50%
10	0.6E-07			1.09E-07		
20	0.30E-07	1.47E-07	1.77E-07	0.55E-07	2.09E-07	3.19E-07
30			1.3E-07			2.70E-07
40			1.2E-07			2.29E-07

	Reduced reaction mechanism			Modified reduced mechanism		
Strain rate $[s^{-1}]$	21%	30%	50%	21%	30%	50%
10	1.23E-07			0.54E-07		
20	0.39E-07	1.20E-06	1.37E-04	0.18E-07	3.62E-07	2.04E-06
30			7.04E-06			1.63E-06
40			5.36E-06			1.30E-06

REFERENCES

[1] Beltrame, A., Porshnev, W., Merchan, W., Saveliev, A., Fridman, A., and Kennedy, A., "Soot and no formation in methane-oxygen enriched diffusion flames," *Combustion and Flame*, vol. 124, pp. 295–310, 2001.

[2] Blazowski, W. *Combustion Science and Technology*, vol. 21, p. 87, 1980.

[3] Bockhorn, H., *Soot formation in combustion: mechanisms and models*. Springer-Verlag, 1994.

[4] Brookes, S. and Moss, J., "Measurements of soot production and thermal radiation from confined turbulent jet diffusion flames of methane," *Combustion and Flame*, vol. 116, pp. 49–61, 1999.

[5] Brookes, S. and Moss, J., "Predictions of soot and thermal radiation properties in confined turbulent jet diffusion flames," *Combustion and Flame*, vol. 116, pp. 486–503, 1999.

[6] Colket, M., Hall, R., and Smooke, M., "Mechanistic models of soot formation," report UTRC93-28, UTRC, 1993.

[7] Frenklach, M. and Harris, S., "Aerosol dynamics modeling using the method of moments," *Journal of Colloid and Interface Science*, vol. 118, no. 1, 1987.

[8] Frenklach, M. and Wang, H., "Detailed modeling of soot particle nucleation and growth," *Twenty-Third Symposium (International) on Combustion, The Combustion Institute*, pp. 1559–1566, 1990.

[9] Frenklach, M. and Wang, H., ch. Soot Formation in Combustion - Mechanisms and Models. Springer, 1994.

[10] Frenklach, M., Wang, H., Goldenberg, M., Smith, G., Golden, D., Bowman, C., Hanson, R., Gardiner, W., and Lissianski, V., "An optimized detailed chemical reaction mechanism for methane combustion," report GRI-95/0058, GRI-Mech, 1995.

[11] Garo, A., Prado, G., and Lahaye, J., "Chemical aspects of soot particles oxidation in a laminar methane-air diffusion flame," *Combustion and Flame*, vol. 79, pp. 226–233, 1990.

[12] Glassman, I., "Soot formation in combustion processes," *Twenty-Second Symposium (International) on Combustion, The Combustion Institute*, pp. 295–311, 1988.

[13] Kennedy, I., Kollmann, W., and Chen, Y. *AIAA Journal*, vol. 29(9), p. 1452, 1991.

[14] Kronenburg, A., Bilger, R., and Kent, J., "Modeling soot formation in turbulent methane-air jet diffusion flames," *Combustion and Flame*, vol. 121, pp. 24–40, 2000.

[15] Law, C., Sung, C., Yu, G., and Axelbaum, R., "On the structural sensitivity of purely strained planar premixed flames to strain rate variations," *Combustion and Flame*, vol. 98, pp. 139–154, 1994.

[16] Lee, K., Thring, M., and Beer, J., "On the rate of combustion of soot in a laminar soot flame," vol. 6, pp. 137–145, 1962.

[17] Leung, K. and Lindstedt, P., "A simplified reaction mechanism for soot formation in non-premixed flames," *Combustion and Flame*, vol. 87, pp. 289–305, 1991.

[18] Lindstedt, P., "A reaction mechanism for soot formation in non-premixed flames," *Proceedings of the IUTAM Symposium on Aerothermodynamics in Combustions*, pp. 145–158, 1992.

[19] Lindstedt, P., *Soot Formation in Combustion-Mechanisms and Models(H.Bockhorn, Ed.)*, ch. Simplified Soot Nucleation and Surface Growth Steps for Non-Premixed Flames. Springer, 1994.

[20] Lutz, A., R.J. Kee, R., Grcar, J., and Rupley, F., *OPPDIF: A Fortran Program for Computing Opposed-Flow Diffusion Flames*. Sandia National Laboratories, sand96-8243 ed., 1997.

[21] Miller, J. and Melius, C., "Kinetic and thermodynamic issues in the formation of aromatic compounds in flames of aliphatic fuels," *Combustion and Flame*, vol. 91, pp. 21–39, 1992.

[22] Miller, J., Honnery, D., and Kent, J. *Twenty-Fourth Symposium (International) on Combustion, The Combustion Institute*, pp. 1031–1039, 1992.

[23] Miller, W., Calcote, H., Olson, D., and Kell, D., "Ionic mechanisms of carbon formation in flames," *Energy and Fuels*, vol. 2, p. 494, 1988.

[24] Moss, J., Stewart, C., and Syed, K., "Flowfield modelling of soot formation at elevated pressure," *Twenty-Second Symposium (International) on Combustion, The Combustion Institute*, p. 413, 1988.

[25] Puri, I., Seshadri, K., Smooke, M., and Keyes, D. *Combustion Science and Technology*, vol. 56, pp. 1–22, 1987.

[26] Santoro, R., Yeh, T., Horvath, J., and Senerjian, H., "The transport and growth of soot particles in laminar diffusion flames," *Combustion Science and Technology*, vol. 53, pp. 89–115, 1987.

[27] Sivathanu, Y. and Gore, J. *Combustion and Flame*, vol. 110, pp. 256–263, 1997.

[28] Smooke, M., Puri, I., and Seshadri, K. *Twenty-First Smyposium (International) on Combustion, The Combustion Institute*, pp. 1783–1792, 1986.

[29] Smyth, K., Miller, J., Dorfman, R., Mallard, W., and Santoro, R., "Soot inception in a methane/air diffusion flame as characterized by detailed species profiles," *Combustion and Flame*, vol. 62, pp. 157–181, 1985.

[30] Street, J. and Thomas, A. *Fuel*, vol. 34, p. 4, 1955.

[31] Sung, C. Private Communication.

[32] Sung, C., Law, C., and Chen, J., "An augmented reduced mechanism for methane oxidation with comprehensive global parametric validation," *Twenty-Seventh Symposium (International) on Combustion, The Combustion Institute*, pp. 295–304, 1998.

[33] Takahashi, F. and Glassman, I. *Combustion Science and Technology*, vol. 37, p. 1, 1984.

[34] Tesner, P., Snegiriova, T., and Knorre, V. *Combustion and Flame*, vol. 17, p. 253, 1971.

[35] Turns, S., *An Introduction to Combustion: Concepts and Applications*. The McGraw - Hill, 2nd ed., 2000.

[36] Vandsburger, U., Kennedy, I., and Glassman, I., "Sooting counterflow diffusion flames with varying oxygen index," *Combustion Science and Technology*, vol. 39, pp. 263–285, 1984.

[37] Vandsburger, U., Kennedy, I., and Glassman, I. *Twentieth Symposium (International) on Combustion, The Combustion Institute*, p. 1105, 1985.

[38] Vincitore, A. and Senkan, A. *Combustion Science and Technology*, vol. 130, pp. 233–246, 1997.

[39] Wang, H., Du, D., Sung, C., and Law, C., "Experiments and numerical simulation on soot formation in opposed-jet ethylene diffusion flames," *Twenty-Sixth Symposium (International) on Combustion, The Combustion Institute*, pp. 2359–2368, 1996.

[40] Wang, H. and Frenklach, M. in press.

[41] Wang, H. and Frenklach, M., "A detailed kinetic modeling study of aromatics formation in laminar premixed acetylene and ethylene flames," *Combustion and Flame*, vol. 110, pp. 173–221, 1997.

[42] Wolfhard, H. and Parker, W. *Proc. Phys. Soc.*, vol. A65, p. 2, 1952.

[43] Wright, W. *Twelfth Symposium (International) on Combustion, The Combustion Institute*, p. 867, 1969.